6
Restricted diffusion

In 1963, Donald Woessner [1] carried out a series of steady gradient spin-echo experiments in samples comprising small solvent molecules in the presence of a solid matrix, in each case varying the gradient amplitude at fixed echo time, τ, so that for each value of τ, an apparent diffusion coefficient was obtained from the normalised echo amplitude relation

$$E = \exp(-\tfrac{2}{3}\gamma^2 g^2 D_{\rm app}\tau^3) \tag{6.1}$$

Woessner found that $D_{\rm app}$ was a function of the echo time, decreasing as τ increased. In particular for liquid water molecules in the presence of a solid silica suspension or imbibed in a porous sandstone matrix, the rate of decay of $D_{\rm app}$ with respect to τ depended on the nature of the sample microstructure, while the value of $D_{\rm app}$ appeared to extrapolate back to the molecular self-diffusion D_0, as $\tau \to 0$. What Woessner had shown was that gradient spin-echo NMR was an effective tool for measuring restricted diffusion, and that the separate dependencies of echo amplitude on echo time and applied gradient allowed access to more subtle features of the translational dynamics.

Over the next two decades, the use of PGSE NMR to detect the influence of geometric restrictions to free diffusion largely centred on the time-dependent apparent diffusion effect, the relevant dimensionless parameter being the ratio of the diffusion length associated with the diffusion encoding time Δ to the characteristic structural length, l_s, the mean distance between diffusive barriers. For $(D_0\Delta)^{1/2}/l_s \ll 1$, unrestricted self-diffusion was observed, while for $(D_0\Delta)^{1/2}/l_s \gg 1$, $D_{\rm app} \to 0$ in the case of molecules completely enclosed by pores, or, where an interconnected pathway allowed molecules to diffuse around and between the barriers, $D_{\rm app}$ settled to some reduced asymptotic value.

The first indications that a richer seam of information could be mined from the PGSE NMR experiment were apparent in the deviation of the echo decays from the simple Stejskal–Tanner expression, often found in restricted diffusion experiments. The functional dependence of $E(g, \Delta)$ commonly resembled a linear superposition of Gaussians, for example in the case of samples comprising an isotropic distribution of liquid-crystalline domains in which the local diffusion is restricted in only one or two dimensions.

In this chapter we examine in detail the effects of restricted diffusion on the PGSE NMR signal. The phenomenology is complicated, or perhaps enriched, by the role of surface relaxation of spin magnetisation as molecules collide with boundaries, and by the influence on diffusing spins of magnetic field inhomogeneities resulting from susceptibility differences between the fluid and the solid matrix. And the influence of all these effects is highly dependent on the nature of the gradient waveform. We will

Translational Dynamics and Magnetic Resonance, First Edition, Paul T. Callaghan, © Paul T. Callaghan 2011.
Published in 2011 by Oxford University Press.

find that the subject matter is sufficiently complicated that no general mathematical solution can be found to satisfy all conditions. Rather, the art of the experimenter is to devise the gradient waveform best suited to elucidating the structural and dynamical parameters of interest, and to choose the theoretical framework which most aptly describes that choice.

We begin by defining what we mean by a diffusion coefficient, in the contexts both of the NMR measurement and the physics of the molecular ensemble. Having done so, we then focus our attention on the diffusive behaviour of liquid molecules in a porous medium, independently of the NMR measurement. Next, the effect of bounding surfaces on spin relaxation is considered, followed by a discussion of the effect of susceptibility inhomogeneity on both the NMR free-induction decay and spin echo, as a result of molecular migration in the resulting inhomogeneous magnetic field. Finally we turn to the PGSE NMR experiment, in which external pulsed gradients are applied, allowing for relaxation and inhomogeneous local fields where appropriate and tractable.

6.1 Apparent and effective diffusion coefficients

Woessner's measured diffusion coefficient, D_{app}, was the value of the diffusion parameter needed to fit the data for his steady gradient spin-echo experiment. In magnetic resonance measurements of diffusion using magnetic field gradients and echoes, the term *apparent diffusion coefficient*, or ADC as it is known in the MRI literature, is a parameter intimately related to the particular echo method used to measure diffusion, and to the representation of that method by some suitable echo-attenuation expression parametrised by some D value. These expressions are largely based on a Fickian assumption of unrestricted self-diffusion in which the distribution of displacements is Gaussian and the mean-squared displacement is proportional to time. In that case, D_{app} properly represents the molecular self-diffusion coefficient. But where diffusion is restricted by surfaces or boundaries, these simple expressions no longer apply, so that while one might fit some parameter D_{app}, its value may depend on the strength of the gradient or the echo time used in that particular measurement. Consequently, its precise meaning may be obscure [2].

From a molecular standpoint, we may unequivocally declare what we mean by a diffusion coefficient, even where restricted diffusion applies. To do so, we simply return to the Einstein definition of eqn 1.44, in which D relates to the time dependence of mean-squared displacement. That relationship provides a working definition of a D value, even where the distribution is no longer Fickian. That value can be termed an *effective diffusion coefficient*, D_{eff}, and in the next section we show how that definition applies where diffusion is restricted.

Given the uncertainty surrounding D_{app}, how might we use gradient echo methods to yield parameters that relate directly to well-understood molecular quantities? First, it helps if we can model the system under study in a manner that is reflected in more appropriate echo-attenuation expressions than those based on a naive application of Fick's law! But even where we are unable to know in advance the relevant physics for our system, the magnetic resonance measurement can provide unambiguous molecular insight. First, in the case of the narrow gradient pulse version of the PGSE NMR

experiment, the low q limit returns the mean-squared displacement corresponding to a migration time Δ, so that in this case $D_{\text{app}} = D_{\text{eff}}$. Second, in the steady gradient CPMG experiment described in Section 5.7.2, eqn 5.146 tells us that the measurement returns $D(\omega)$, where $\omega = 2\pi/T$, T being the period repeat interval. This $D(\omega)$ is precisely the spectral component of the molecular velocity autocorrelation function, as defined by eqn 5.132.

6.2 Time-dependent mean-squared displacement

The simplest probe of restricted diffusion involves a measurement of the effective diffusion coefficient, $D_{\text{eff}}(t)$, as a function of the diffusion time, where, using the Einstein definition,

$$D_{\text{eff}}(t) = \frac{\langle(\mathbf{r}(t) - \mathbf{r}(0))^2\rangle}{6t} \tag{6.2}$$

In the limit as $t \to 0$, the diffusion coefficient for most of the molecules in a fluid with bounding walls will be the free molecular diffusion coefficient D_0. However, for a small fraction of molecules, close to the walls, diffusion is inhibited. How big that fraction is, and how much the diffusion is inhibited, we consider in the following sections. For the moment, however, we will take a coarse view in which our description will be dominated by molecules in the bulk.

Suppose the mean distance between walls is given by some length scale d. d might be a typical pore diameter in the case of a porous medium. Fig. 6.1 illustrates the effect of collision with the boundaries as the diffusion time is increased. At times sufficiently small that few molecules collide with the boundaries, $\langle(\mathbf{r}(t)-\mathbf{r}(0))^2\rangle$ increases linearly with time, with a slope corresponding to the free molecular self-diffusion coefficient, D_0. At longer times, wall collisions cause the diffusion coefficient to reduce, and for times $t \gg d^2/6D_0t$, the diffusion coefficient becomes zero in the case of isolated pores, with $\langle(\mathbf{r}(t) - \mathbf{r}(0))^2\rangle$ limiting at a value on the order of d^2. By contrast, for interconnected pores, the diffusion coefficient reaches an asymptotic value $D_{\text{eff}}(\infty)$, reduced from the free diffusion coefficient by tortuosity effects, but nonetheless finite.

6.2.1 Tortuosity and the long-time limit

Tortuosity is a measure of the pore connectivity in an interconnected porous medium. The tortuosity, α, is defined by the relation [3]

$$\lim_{t\to\infty} \frac{D_{\text{eff}}(t)}{D_0} = \frac{D_{\text{eff}}(\infty)}{D_0} = \frac{1}{\alpha} \tag{6.3}$$

In simple model systems, for example randomised bead packs, α may be calculated as $\phi^{-1/2}$ [4], where ϕ is the volume fraction of the pore space. However, in more complex porous structures, such a simple relationship breaks down and α is traditionally measured from the 'formation factor'

$$\frac{1}{F} = \frac{\sigma_p}{\sigma_0} \tag{6.4}$$

where σ_0 and σ_p are the respective electrical conductivities for an electrolyte solution in the bulk and in the case where the solution fills the porous medium. Then $\alpha = F\phi$ [5] and

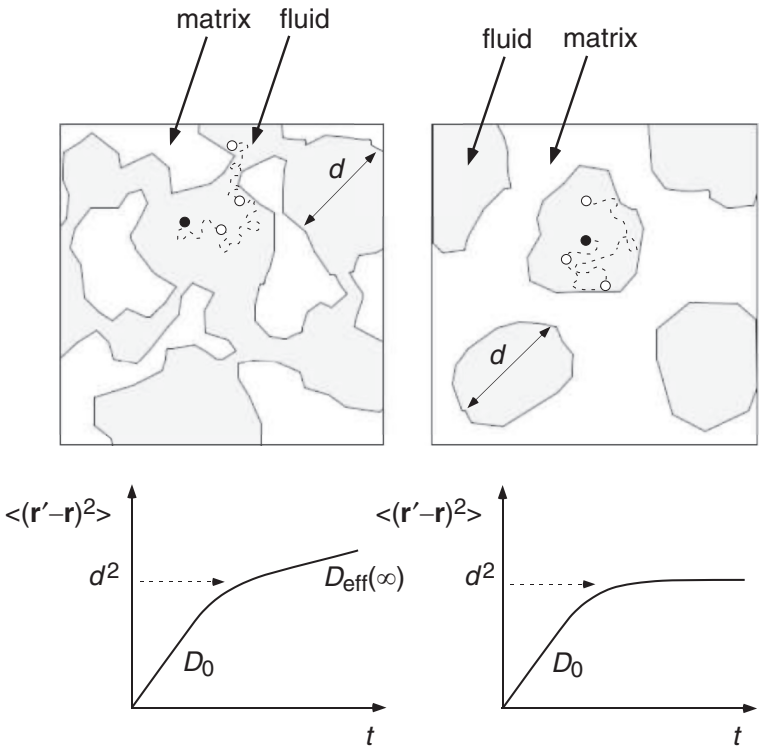

Fig. 6.1 Schematic representation of time-dependent diffusion in an interconnected porous medium (left) and in a system of isolated pores (right).

$$\frac{D_{\text{eff}}(\infty)}{D_0} = \frac{1}{F\phi}. \tag{6.5}$$

The approach to asymptotic conditions can be sufficiently gradual that the determination of $D_{\text{eff}}(\infty)$ may be difficult in practice. There is broad agreement [6, 7] that this approach may be represented as

$$\frac{D_{\text{eff}}(t)}{D_0} = \frac{1}{\alpha} + \frac{\beta_1}{t} - \frac{\beta_2}{t^{3/2}} \tag{6.6}$$

Presumably, there exists some macroscopic length scale, $L_{macro} \sim REV^{1/3}$ (see Section 2.3.2), such that molecules must diffuse a distance L_{macro} in order to reach the asymptotic limit. On that basis Mair *et al.* [8] have proposed $\beta_1 \sim L^2_{macro}/D_0 t$.

The narrow gradient pulse PGSE NMR experiment is ideally suited to the measurement of $D_{\text{eff}}(t)$, the low q-response yielding the molecular mean-squared displacements directly. At finite q, a much more complex behaviour of the echo attenuation is found. These effects, along with their dependence on the actual gradient waveform, will be discussed in later sections. For the moment, we turn our attention from the the long-time behaviour to the short-time response of $D_{\text{eff}}(t)$.

6.2.2 The short-time limit for restricted diffusion

The indication that a layer of molecules near the boundaries of a porous medium experience inhibited diffusion is dramatically demonstrated in NMR microimaging experiments. Because MRI experiments are generally performed using a spin echo, the effect of diffusion under the influence of the imaging gradients is to cause an attenuation of the image, this attenuation becoming severe when the diffusion distance over the echo time is comparable with the dimension of an imaging voxel [9]. Figure 6.2 shows a high-resolution proton NMR image of water in a 1.9 mm inner-diameter capillary tube, in which a crescent of enhancement is seen due to the effect of the read gradient attenuating the NMR signal from molecules diffusing in the horizontal direction.

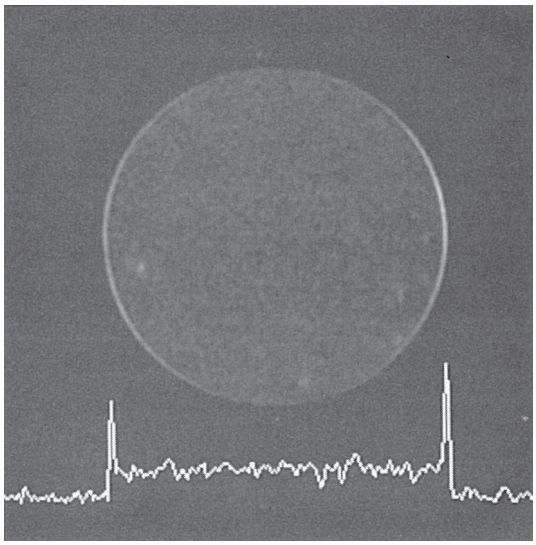

Fig. 6.2 Proton NMR microimage of a 1.9 mm inner diameter water filled capillary, showing edge enhancement where molecular diffusion along the read gradients direction is restricted by the walls. (Reproduced by permission from reference [9].)

The thickness of the restricted layer is on the order of the rms diffusion distance, $(D_0 t)^{1/2}$, when the characteristic measurement time is t. Thus the proportion of fluid experiencing the restriction on a wall of surface area S for an enclosing pore will be approximately $S(D_0 t)^{1/2}/V_p$, where V_p is the pore volume. By this simple scaling argument, we might expect that the short-time behaviour of the diffusion will follow

$$\frac{D_{\text{eff}}(t)}{D_0} = 1 - \frac{(D_0 t)^{1/2} S}{V_p} \tag{6.7}$$

An exact solution to this problem was found in a very elegant manner by Mitra and co-workers [10, 11], who obtained a result

$$\frac{D_{\text{eff}}(t)}{D_0} = 1 - \frac{4\sqrt{D_0 t}}{9\sqrt{\pi}} \frac{S}{V_p} + \mathcal{O}(D_0 t) \tag{6.8}$$

which, remarkably, holds for any pore shape, provided that the pore walls are smooth. Their derivation is based on a careful consideration of the behaviour of the diffusion probability distribution in the vicinity of the wall.

When diffusing near an impermeable boundary, molecules colliding with the wall are reflected. To understand this process quantitatively it is helpful to return to the conditional probability, $P(\mathbf{r}|\mathbf{r}', t)$, where $\mathbf{r}$ and $\mathbf{r}'$ represent the respective start and finish coordinates[1] of the diffusing molecule, and t is the time over which we will measure diffusion. Diffusing molecules will be aware of the wall only if their starting distance from the wall is not much greater than $2D_0t$. We will treat the wall as smooth, in other words flat over the length $2D_0t$. Since we are interested in the limiting case $t \to 0$, this flatness condition will always apply, unless the wall geometry is fractal. Suppose we represent the displacement normal to the wall by x. That means the range of x is from 0 to ∞, the latter meaning any distance much larger than the diffusion length $2D_0t$. y and z, by contrast, will range from $-\infty$ to ∞.

The effect of the reflective boundary condition is such that we can represent the conditional probability for molecules starting at (x, y, z) by including in addition an identical image displaced beyond the wall at $(-x, y, z)$, as shown in Fig. 6.3. Hence the apparent diffusion coefficient measured over time t will be simply obtained.

In the following derivation, we assume pore volume V_p and hence a uniform pore density function V_p^{-1}. The integration of y and z over the range $-\infty$ to ∞ will be equivalent to integrating over any surface area ΔS where the extent of the area in the y and z directions exceeds $2D_0t$. Given $t \to 0$ then we can conveniently choose ΔS sufficiently small that no pore surface curvature effects need be considered. The elements, ΔS and $\Delta V_p = \Delta S \int_0^\infty dx$ can then be summed to encompass the entire pore surface area, S, and volume, V_p.

We start by evaluating the mean-squared displacement over time t,

$$\langle(\mathbf{r}' - \mathbf{r})^2\rangle = \int\int \rho(\mathbf{r}) P(\mathbf{r}|\mathbf{r}', t)(\mathbf{r}' - \mathbf{r})^2 d\mathbf{r}' d\mathbf{r}. \tag{6.9}$$

Including the image term in $P(\mathbf{r}|\mathbf{r}', t)$, we have

$$\begin{aligned}\langle(\mathbf{r}' - \mathbf{r})^2\rangle = \frac{1}{V_p} \int_{-\infty}^{\infty} dz \int_{-\infty}^{\infty} dz' \int_{-\infty}^{\infty} dy \int_{-\infty}^{\infty} dy' \int_0^{\infty} dx \int_0^{\infty} dx' \\ \times \frac{1}{(4\pi D_0 t)^{3/2}} \exp(-\frac{(z'-z)^2}{4D_0t}) \exp(-\frac{(y'-y)^2}{4D_0t}) \\ \times [\exp(-\frac{(x'-x)^2}{4D_0t}) + \exp(-\frac{(x'+x)^2}{4D_0t})] \\ \times [(x'-x)^2 + (y'-y)^2 + (z'-z)^2]\end{aligned} \tag{6.10}$$

[1] In other words $\mathbf{r}(0)$ and $\mathbf{r}(t)$ of our previous notation.

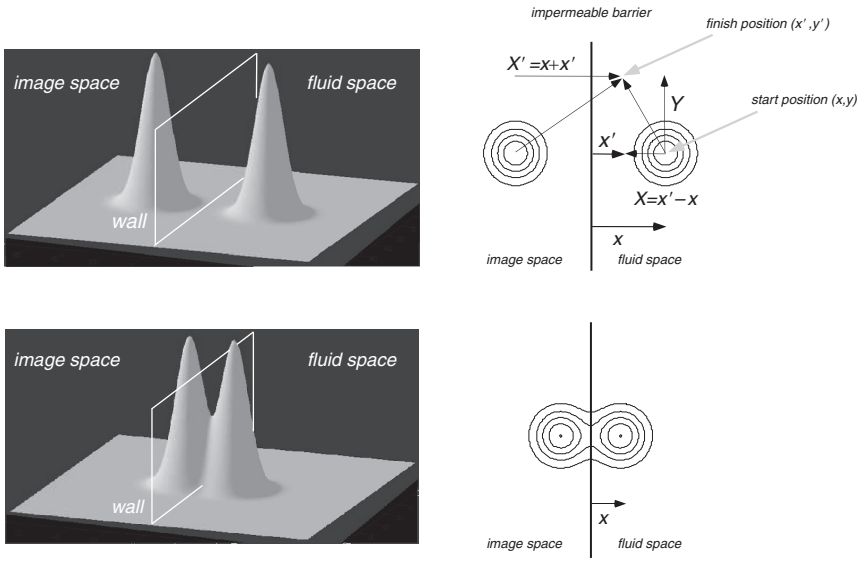

Fig. 6.3 The effect of diffusion in the vicinity of a smooth impermeable barrier in which diffusing particles are reflected at the wall. The process can be represented by adding to the Gaussian conditional probability for diffusion an image Gaussian in the space beyond the wall. The upper diagrams show a 2-D representation of the behaviour when the starting displacement from the wall, x is much larger than $2D_0t$, while the lower diagram shows the case $x \sim 2D_0t$. Note the definition of coordinates, where X and Y represent the displacement from origin (x, y) to position (x', y') at time t.

and hence

$$\begin{aligned}\langle(\mathbf{r}'-\mathbf{r})^2\rangle = \frac{1}{V_p}\int_{-\infty}^{\infty}dz\int_{-\infty}^{\infty}dZ\int_{-\infty}^{\infty}dy\int_{-\infty}^{\infty}dY\int_{0}^{\infty}dx\int_{-x}^{\infty}dX \\ \times\frac{1}{(4\pi D_0t)^{3/2}}[\exp(-\frac{X^2}{4D_0t})\exp(-\frac{Y^2}{4D_0t})\exp(-\frac{Z^2}{4D_0t}) \\ \times(X^2+Y^2+Z^2) \\ +[\exp(-\frac{(X+2x)^2}{4D_0t})\exp(-\frac{Y^2}{4D_0t})\exp(-\frac{Z^2}{4D_0t})\exp(-\frac{X^2}{4D_0t}) \\ \times(X^2+Y^2+Z^2)] \\ = 6D_0t-\frac{S}{V_p}\frac{1}{(4\pi D_0t)^{1/2}}\int_0^{\infty}dx\int_{-\infty}^{-x}dX(X^2+4D_0t) \\ +\frac{S}{V_p}\frac{1}{(4\pi D_0t)^{1/2}}\int_0^{\infty}dx\int_x^{\infty}dX'((X'-2x)^2+4D_0t)\exp(-\frac{(X')^2}{4D_0t})\end{aligned} \tag{6.11}$$

where $X' = (x + x') = X + 2x$. The remaining part of the derivation requires careful successive integration by parts, leading finally to

$$\langle(\mathbf{r}'-\mathbf{r})^2\rangle = 6D_0t - 4\frac{(2D_0t)^2}{(4\pi D_0t)^{1/2}}\frac{S}{V_p} + \frac{1}{(4\pi D_0t)^{1/2}}\frac{S}{V_p}\int_0^\infty 4x^2\int_x^\infty \exp(-\frac{X^2}{4D_0t}) \quad (6.12)$$

Again integrating by parts, the last double integral is easily shown to be equivalent to $8(2D_0t)^2/3$, whence

$$\langle(\mathbf{r}'-\mathbf{r})^2\rangle = 6D_0t - \frac{4(2D_0t)^2}{3(4\pi D_0t)^{1/2}}\frac{S}{V_p} \quad (6.13)$$

The effective diffusion coefficient, $D_{\text{eff}}(t)$, is given by $\langle(\mathbf{r}'-\mathbf{r})^2\rangle/6t$ and, normalised to the molecular self-diffusion coefficient, yields

$$\lim_{t\to 0}\frac{D_{\text{eff}}(t)}{D_0} = 1 - \frac{4\sqrt{D_0t}}{9\sqrt{\pi}}\frac{S}{V_p} \quad (6.14)$$

6.2.3 Interpolation of short- and long-time limits for restricted diffusion

Having expressions for both the short- and long-time limits for $D_{\text{eff}}(t)/D_0$, the Pade approximant [12] can be used to interpolate. A Pade approximant is the 'best' approximation of a function by a rational function of given order. In the present case, a two-point approximant (agreement as $t \to 0$ and $t \to \infty$) gives [13]

$$\frac{D_{\text{eff}}(t)}{D_0} = 1 - (1-\frac{1}{\alpha})\,\frac{c\sqrt{t} + (1-1/\alpha)t/\theta}{(1-1/\alpha) + c\sqrt{t} + (1-1/\alpha)t/\theta} \quad (6.15)$$

where $c = (4/9\sqrt{\pi})(S/V_p)(\sqrt{D_0})$ and θ is a parameter with dimensions of time. Gas and water diffusion experiments [8, 13] in monodisperse bead packs of bead diameter, b, suggest $\sqrt{D_0\theta} \sim 0.14b$. However, for general porous media comprising a wide distribution of pore sizes, θ is a fitting parameter for which no clear geometric relationship has been identified.

Figure 6.4 shows the results of PGSE NMR experiments carried out by Mair *et al.* [8] to measure diffusion for hyperpolarised ^{129}Xe gas at 6.5 bar in a porous medium of pore volume fraction 0.38, comprising randomly packed spherical glass beads of $b = 4$ mm diameter. $D_0 = 8.1 \times 10^{-7}$, and $\sqrt{D_0t} = 0.13b$. The data are plotted as a function of normalised diffusion length $b^{-1}\sqrt{D_0t}$. The tortuosity limit $1/\alpha$ is 0.62, equivalent to the random monodisperse bead pack value $\sqrt{\phi}$ [4], while $bS/V_p = 9.8$, again using the random monodisperse bead pack value, $bS/V_p = 6(1-\phi)\phi$ [13]. The solid line is a Pade approximant fit using eqn 6.15, while the dashed line shows the $\sqrt{D_0t}$-dependence at short times. The fitted value of θ is 0.34 s.

6.2.4 $D_{\text{eff}}(t)$ and calculation of the apparent diffusion coefficient for any gradient waveform

$D_{\text{eff}}(t)$ can be easily measured using the narrow gradient pulse PGSE NMR experiment, where, in the low-q limit, $D_{\text{eff}}(t) = D_{\text{app}}(t)$. For other effective gradient waveforms, a general expression for $D_{\text{app}}(t)$, based on the Gaussian phase approximation and an effective gradient that is piecewise constant in time, has been derived by Zielinski and Sen [14]. Utilising their expression simply requires one to evaluate the integrals

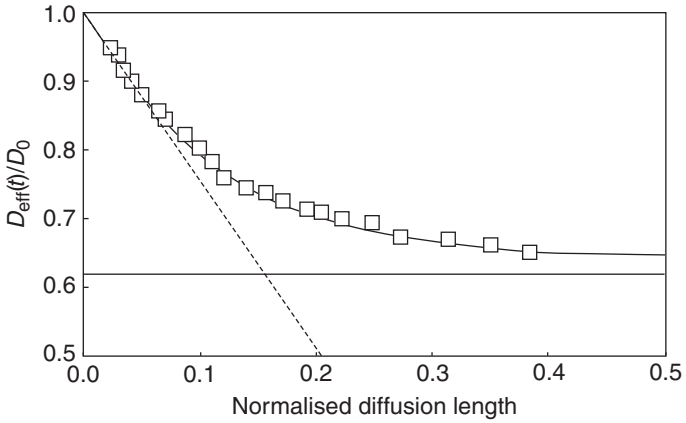

Fig. 6.4 NMR measurements of ^{129}Xe gas (6.5 bar) diffusion in randomly packed spherical glass beads of 4 mm diameter. The solid line is a Pade approximant fit, while the dashed line shows the $\sqrt{D_0 t}$-dependence at short times. (Adapted from Mair *et al.* [8].)

$\int_{t'}^{t''} tD_{\text{eff}}(t)dt$ and $\int_{t'}^{t''} t^2 D_{\text{eff}}(t)dt$, for which the Pade approximant form provides a suitable candidate.

6.2.5 The definition of the asymptotic limit

The discussion of dispersion in Chapter 2 involved a definition (eqn 2.54) of a time-dependent dispersion coefficient expressed in terms of a time derivative of mean-squared displacement. Let us label this case D_{deriv}. By contrast, the effective diffusion coefficient, D_{eff}, defined in eqn 6.2, involves a simple division by time. Clearly the asymptotic behaviours resulting from these two definitions will be very different, as illustrated in Fig. 6.5, where a simple exponential correlation function is used to describe the transition of the rms displacement, $< Z^2(t) >$, from a short-time diffusion coefficient to a long-time value five times smaller.

The question as to which definition of time-dependent diffusion is more appropriate is a matter of standpoint. Of course, just as we define electrical resistance as V/I rather than dV/dI, so we might argue that the basic Einstein definition, involving a simple division of the mean-squared displacement by time, suggests that D_{eff} is the correct choice. It is also the choice that relates directly to the measurement of diffusion by PGSE NMR, since the Stejskal–Tanner equation contains this implicit definitional assumption. However, equally it could be argued that the initial decay of the echo attenuation yields $< Z^2(t) >$ directly, and so, if one is prepared to pay the signal-to-noise ratio price of differentiating experimental data, $D_{\text{deriv}}(t)$ is accessible. Further, the great advantage of $D_{\text{deriv}}(t)$ is that it may be directly identified with the time integral of the velocity autocorrelation function, as in eqn 2.56. This connection to the velocity helps explain why $D_{\text{deriv}}(t)$ is the preferred definition in the physics of dispersion, where particle migration is driven by the flow.

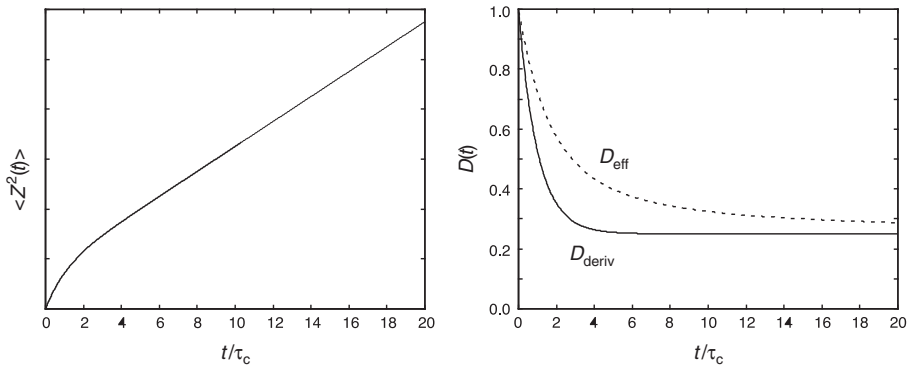

Fig. 6.5 The transition of $\langle Z^2(t)\rangle$, $D_{\rm eff}(t)$, and $D_{\rm deriv}(t)$, from an initial diffusion coefficient $D = 1$ to a final value of $D = 0.2$, illustrating the much more rapid approach to the asymptotic limit of $D_{\rm deriv}(t)$.

So long as one is clear about the choice made and consistent in its use, either $D_{\rm deriv}(t)$ or $D_{\rm eff}(t)$ provide a suitable means of tracking the time dependence of diffusive migration.

6.3 Spin relaxation in microscopically inhomogeneous media

In this section we consider how spin relaxation may be influenced by sample structure and geometry. For the experimentalist wishing to interpret echo-attenuation data, some knowledge of relaxation rates is essential. In PGSE NMR experiments, this knowledge will enable the diffusion observation time, Δ, to be made sufficiently short that relaxation weighting effects can be avoided. Where longer values of Δ are needed, this knowledge might permit interpretation of the echo-attenuation signal using a model that correctly assigns relative weights to signals arising from different local geometries.

The interplay between diffusion and relaxation may be treated in a number of different ways. One simple approach is to assign different relaxation rates to different physical regions of a sample, such that diffusion has the effect of causing molecules to migrate between these different relaxation domains or 'phases'. This perspective, which contains no details of sample geometry, may be termed 'exchange between sites', and is parametrised by assigning relative site occupancies, site residence times, and local site relaxation rates. Exchange theory is the subject of Section 6.3.1.

Another approach is to consider a geometric description in which we distinguish spin relaxation in the bulk liquid phase from that which occurs at the interface with a surrounding solid matrix. For molecules experiencing restricted diffusion in a porous structure, geometry plays an important role in influencing spin relaxation. One relaxation mechanism for spins in pores involves the presence of strong relaxation 'sinks' at the pore surface. These sinks may be due to the presence of paramagnetic centres at the surface or due to local hindering of rotational reorientation allowing an enhanced intra- and inter-molecular dipolar interaction as the liquid molecules are temporarily immobilised. Clearly the ratio of the pore surface to pore volume will vary according to the pore size, so that *a priori* we might expect the overall relaxation behaviour

to be similarly size-dependent. Section 6.3.2 deals with effects deriving from surface collisions.

Near the pore surface, local magnetic field gradients may exist, due to the heterogeneous diamagnetic susceptibility associated with the boundaries. Here, molecular diffusion will result in spin dephasing, an effect which is discussed in Section 6.4.

6.3.1 Exchange between sites

In the exchange model for multi-site relaxation, molecules hop or 'exchange' between sites with different local relaxation rates. The problem is easy to simulate on a computer using Monte Carlo methods. However, the model is amenable to mathematical treatment and is outlined as follows.

Limiting cases for exchange

Exchange may be classified as slow or fast depending on the relative speed of exchange and relaxation. Suppose that the relaxation process is described by an exponential decay of the magnetisation, $M(t)/M_0 = \exp(-t/T)$, where T is the relaxation time such as T_1 ($M(t)$ being the longitudinal magnetisation) or T_2 (with $M(t)$ being the transverse magnetisation). We begin by assigning some characteristic 'exchange time', τ_e, for migration between sites. This set of sites or 'phases' have occupancies P_i, which are taken to be time-independent. Of course $\sum_i P_i = 1$.

Labelling the relaxation time in the ith phase as $T^{(i)}$, [2] then in the slow-exchange case ($T^{(i)} \ll \tau_e$) the total magnetisation relaxation is multi-exponential and given by

$$M(t)/M_0 = \sum_i P_i \exp(-t/T^{(i)}) \tag{6.16}$$

while in fast exchange ($T^{(i)} \gg \tau_e$) a common relaxation is observed for the whole system, with

$$\frac{1}{T} = \sum_i P_i \frac{1}{T^{(i)}} \tag{6.17}$$

For intermediate exchange rates non-exponential relaxation is observed, but the simple subdivision of eqn 6.16 no longer applies.

Intermediate exchange and the Zimmerman–Brittin treatment

Zimmerman and Brittin [15] solved the problem of exchange between sites of differing relaxation rates by defining a probability $P_{ij}(t)$ that a spin initially in the i phase will be found in the j phase a time t later. The Chapman–Kolmogorov equations [16] then require

$$\frac{dP_{ij}(t)}{dt} = -\frac{1}{\tau_j} P_{ij}(t) + \sum_k P_{ik}(t) \frac{1}{\tau_k} p_{kj} \tag{6.18}$$

where $\frac{1}{\tau_k}$ is the probability per second that a spin in the kth phase leaves the kth phase, equivalent to the inverse of the mean k phase residence time for the spin, τ_k.

[2] Note that the superscript labels the site. The relaxation process may be T_1 or T_2 depending on the experiment, in which case, for site i we would have $T_1^{(i)}$ or $T_2^{(i)}$.

p_{kj} is the conditional probability that if a spin leaves the kth phase it will transfer to the jth phase.

Clearly $p_{kk} = 0$ and $\sum_j p_{kj} = 1$. Zimmerman and Brittin then introduce the matrices $\underline{\underline{P}}(t) = [P_{ij}(t)]$ and $\underline{\underline{D}} = [\delta_{ij}\frac{1}{\tau_j} - p_{ij}\frac{1}{\tau_i}]$, and rewrite eqn 6.18 as a matrix equation

$$\dot{\underline{\underline{P}}}(t) = -\underline{\underline{P}}\,\underline{\underline{D}} \tag{6.19}$$

with initial condition $\underline{\underline{P}} = \underline{\underline{1}}$, leading to solution

$$\underline{\underline{P}}(t) = \exp(-\underline{\underline{D}}t) \tag{6.20}$$

The next step is to define the probability $I_{ij}(t)$ of a spin, which started in the i phase, being in the j phase at a later time t, and, in addition, being 'alive'. Hence the differential equation governing I_{ij} not only involves hopping between phases but also the possibility of spin relaxation at rate $1/T^{(j)}$. This leads to an equation similar to eqn 6.18,

$$\frac{dI_{ij}(t)}{dt} = -\frac{1}{\tau_j}I_{ij}(t) - \frac{1}{T^{(j)}}I_{ij}(t) + \sum_k I_{ik}(t)\frac{1}{\tau_k}p_{kj} \tag{6.21}$$

with matrix form

$$\dot{\underline{\underline{I}}}(t) = -\underline{\underline{I}}\,\underline{\underline{F}} \tag{6.22}$$

where $\underline{\underline{F}} = \underline{\underline{D}} + \underline{\underline{E}}$ and $\underline{\underline{E}} = [\delta_{ij}1/T^{(j)}]$. Of course the total signal is simply obtained from the sum

$$\bar{I}(t) = \sum_{i,j} I_{ij}(t)P_i \tag{6.23}$$

In matrix notation

$$\bar{I}(t) = \underline{\tilde{\phi}_0}\,\underline{\underline{I}}\,\underline{\phi_0} \tag{6.24}$$

where $\underline{\tilde{\phi}_0} = [1, 1, 1\ldots]^T$ and $\underline{\phi_0} = [P_1, P_2, P_3 \ldots..]$.

The two-site problem for relaxation

The Chapman–Kolmogorov analysis is particularly simple in the case of exchange between two sites. Since the hopping particles have no choice as to their destination, $p_{12} = 1$ and

$$\underline{\underline{D}} = \begin{bmatrix} 1/\tau_1 & -1/\tau_1 \\ -1/\tau_2 & 1/\tau_2 \end{bmatrix} \tag{6.25}$$

and

$$\underline{\underline{D}}^2 = (\frac{1}{\tau_1} + \frac{1}{\tau_2})\underline{\underline{D}} \tag{6.26}$$

from which all powers of $\underline{\underline{D}}$ may be obtained, resulting in

$$\begin{aligned} \underline{\underline{P}} &= \exp(-\underline{\underline{D}}t) \\ &= \underline{\underline{1}} + \frac{e^{-\lambda t} - 1}{\lambda}\underline{\underline{D}} \end{aligned} \tag{6.27}$$

where

$$\lambda = 1/\tau_1 + 1/\tau_2 \tag{6.28}$$

This defines an effective exchange time $\tau_e = \lambda^{-1}$.

Of course the steady-state occupancies, P_1 and P_2, are defined by the ratio of the rates $1/\tau_1$ and $1/\tau_2$. Given that constraint, eqn 6.27 is equivalent to

$$\begin{aligned} P_{11} &= P_1 + P_2 \exp(-\lambda t) \\ P_{12} &= P_2 - P_2 \exp(-\lambda t) \\ P_{21} &= P_1 - P_1 \exp(-\lambda t) \\ P_{22} &= P_2 + P_1 \exp(-\lambda t). \end{aligned} \tag{6.29}$$

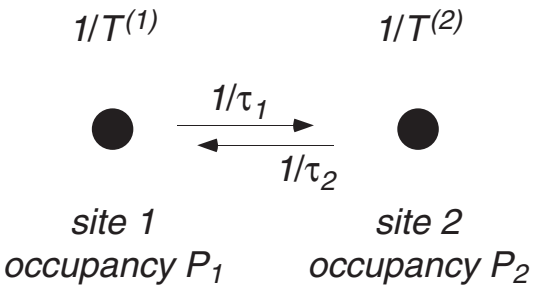

Fig. 6.6 Schematic representation of two-site exchange with local relaxation rates $1/T^{(1)}$ and $1/T^{(2)}$.

The Zimmerman–Brittin solution to the relaxation problem for two-site exchange is equally simple, with the matrix $\underline{\underline{F}}$ given by

$$\underline{\underline{F}} = \begin{bmatrix} 1/\tau_1 + 1/T^{(1)} & -1/\tau_1 \\ -1/\tau_2 & 1/\tau_2 + 1/T^{(2)} \end{bmatrix} \tag{6.30}$$

with eigenvalues

$$\lambda_1, \lambda_2 = \frac{1}{2}\left\{ \frac{1}{T^{(1)}} + \frac{1}{T^{(2)}} + \frac{1}{\tau_1} + \frac{1}{\tau_2} \mp \left[\left(\frac{1}{T^{(2)}} - \frac{1}{T^{(1)}} + \frac{1}{\tau_2} - \frac{1}{\tau_1} \right)^2 + \frac{4}{\tau_1 \tau_2} \right]^{1/2} \right\} \tag{6.31}$$

and solution

$$\bar{I}(t) = a_1 \exp(-\lambda_1 t) - a_2 \exp(-\lambda_2 t) \tag{6.32}$$

where

$$\begin{aligned} a_1 &= \frac{1}{\lambda_2 - \lambda_1}[\lambda_2 - 1/T^{(av)}] \\ a_2 &= \frac{1}{\lambda_2 - \lambda_1}[\lambda_1 - 1/T^{(av)}] \end{aligned} \tag{6.33}$$

and

$$1/T^{(av)} = P_1/T^{(1)} + P_2/T^{(2)}. \tag{6.34}$$

Strictly speaking, the requirement for slow exchange is that $1/\tau_1 \ll 1/T^{(1)}$ and $1/\tau_2 \ll 1/T^{(2)}$, while for fast exchange, $1/\tau_e = 1/\tau_1 + 1/\tau_2 \gg 1/T^{(1)}$ *and* $1/T^{(2)}$

suffices. Of course, the fast-exchange description is too simplistic when τ_e becomes comparable with the correlation time governing the relaxation process and relaxation and exchange processes become coupled. A more general treatment of such exchange has been discussed in detail by Wennerstrom [17].

Bound water and exchange

One simple example of two-site exchange concerns the migration of water molecules between 'bound' and 'free' states. The rotational correlation time for free water is around 10^{-12} s [18]. 'Bound water' is an ill-defined term, generally used to describe water molecules closely associated with larger molecules or with solid surfaces, and having much slower tumbling rates, with rotational correlation times typically 10^{-8} s [19]. One indication that bound water is structurally modified comes from the depression of the freezing point, an effect apparent in an NMR experiment by the persistence of a liquid-like signal at temperatures below 0°C [20–22]. The question of 'structure' in bound water is a contentious topic that need not concern us [23]. Nonetheless it is clear that at least two phases of water—bound and free—exist in biological tissue, as well as in mineral systems, where there are solid surfaces with which the water can interact.

The slowing of rotational motion in the bound phase leads to a reduction in both T_1 and T_2 until the correlation time for dipolar fluctuation is of order the Larmor period of around 10^{-9} s. This is the characteristic T_1 minimum apparent in Fig. 4.15, and for a proton pair undergoing isotropic motion, the relaxation values at this minimum ($\omega_0\tau_c \sim 1$) are of order 10–100 ms for $\omega_0 \sim 100$ MHz. At slower tumbling rates, T_2 continues to fall while T_1 increases. The slowing of reorientational motion in the 'bound' water molecule will inevitably lead to altered proton relaxation for the entire water system, in accordance with the model of Zimmerman and Brittin [15]. The reader is referred to the excellent reviews on the subject of water relaxation [24–27].

Note that the mean time taken for a proton to 'sample' the differing water phases, the exchange correlation time, τ_e, may be due to molecular diffusion or via chemical exchange of protons between adjacent water molecules. While chemical exchange can be important for short-range processes, it is quite slow, taking on the order of'milliseconds per jump, so that the dominant process determining the rate of translation between spatially separated regions is molecular self-diffusion.

Equation 6.17 leads to a fast-exchange result for bound and free water,

$$\frac{1}{T_1} = \left(\frac{1}{T_1}\right)_f + P_b\{\left(\frac{1}{T_1}\right)_b - \left(\frac{1}{T_1}\right)_f\} \tag{6.35}$$

The second term in eqn 6.18 is generally dominant when the bound water correlation time is small [28, 29], leading to a simple proportionality between the T_1 relaxation rate and the bound fraction, P_b [30]. This is a very useful relationship since it indicates that over a narrow composition range, T_1 should be approximately proportional to water content.

It is clear that in biological samples the transition between the bound and free water is not sharp, so that a two-phase description is simplistic. This means that there is seldom a single characteristic exchange time, but rather a continuous spectrum [18, 31].

A variety of correlation time distribution models, applicable to biological tissues, is available [32–34]. Because of the role of diffusion in determining transfer between phases, the exchange process will also be strongly influenced by geometry. In the next section we discuss spin relaxation in the context of diffusion between the bulk and the surrounding surface on which 'relaxation sinks' are present. This model can be used to explain relaxation of water in plant cell and animal cells, but is particularly important in porous mineral structures such as clays and sandstones.

6.3.2 Relaxation sinks and normal modes: wall relaxation and the Brownstein–Tarr relations

We now return to the problem of surface relaxation for molecules experiencing restricted diffusion in a porous structure. The problem has been treated in detail by Brownstein and Tarr [35], who adopt the classical 'magnetisation diffusion' approach of Bloch and Torrey in assigning a magnetisation density, $M(\mathbf{r}, t)$, that obeys the Fick's Law differential equation

$$D\nabla^2 M(\mathbf{r}, t) = \frac{\partial M(\mathbf{r}, t)}{\partial t}. \tag{6.36}$$

The treatment is exactly as in Chapter 1, where the diffusion of molecular probability density was described. Now $M(\mathbf{r}, t)$ describes the combined probability of finding the molecule at $(\mathbf{r}, t)$ such that its spin has not relaxed. $M(\mathbf{r}, t)$ could refer to the longitudinal magnetisation, in the case of T_1 relaxation, or transverse magnetisation, in the case of T_2. Just as we saw in Chapter 1, for the case of collision with partially absorbing walls, for walls that partially relax the magnetisation,

$$D\hat{\mathbf{n}} \cdot \nabla M(\mathbf{r}, t) + \bar{\rho} M(\mathbf{r}, t))|_S = 0 \tag{6.37}$$

where $\bar{\rho}$ is the surface relaxivity parameter. The effect of bulk relaxation can be ignored for the moment as it simply adds an additional fixed relaxation decay to the problem. Equation 6.36 applies within the volume of a pore and reflects the transport of magnetisation via the diffusion of the molecules. Equation 6.37 is the boundary condition on the pore surface, taking into account the sink.

The general solution to eqn 6.36 can be written [36]

$$M(\mathbf{r}, t) = \sum_{n=0}^{\infty} a_n u_n(\mathbf{r}) \exp(-t/T_n) \tag{6.38}$$

where u_n and T_n are eigenfunctions and eigenvalues of the Helmholtz equation

$$u_n/T_n + D\nabla^2 u_n = 0 \tag{6.39}$$

with boundary condition

$$D\hat{\mathbf{n}} \cdot \nabla u_n(\mathbf{r}) + \bar{\rho} u_n(\mathbf{r})|_S = 0 \tag{6.40}$$

The solution takes the form of a sum of normal modes that will depend on the geometry and on the sink strength, $\bar{\rho}$. The eigenfunctions $u_n(\mathbf{r})$ may be normalised with respect to an integration over the pore volume V by $(1/V) \int d\mathbf{r} u_n^2 = 1$.

This generalised solution will prove to be useful in discussing 2-D relaxation experiments in Chapter 9. For the moment, however, we will return to the original notation of Brownstein and Tarr, in which the relaxation of the signal $M(t)$ is obtained by equating $M(t)$ with $\int_V M(\mathbf{r},t)d\mathbf{r}$, and allowing the initial condition $M(\mathbf{r},0) = M(0)/V$. The form of the normal modes solution was written by these authors as

$$M(t) = M(0)\sum_{n=0}^{\infty} I_n \exp(-t/T_n) \tag{6.41}$$

The connection with eqn 6.38 is obvious, with $I_n = a_n \int_V d\mathbf{r} u_n$.

Equation 6.41 can describe either the T_1 or T_2 relaxation process, depending on the value of $\bar{\rho}$ chosen. The parameters that determine I_n and T_n are the molecular self-diffusion coefficient, D, the pore size, a, and the average sink strength, $\bar{\rho}$, over the pore surface. This latter parameter is somewhat empirical and a variety of methods are employed in its estimation. Of course, the interesting feature of the normal modes is their dependence on pore size. Solutions are as follows:

(a) Planar geometry (bounded by $z = -a$ and $z = a$)[3]

$$\begin{aligned} I_n &= \frac{4\sin^2(\xi_n)}{2\xi_n^2 + \xi_n \sin(2\xi_n)} \\ T_n &= \frac{a^2}{D\xi_n^2} \end{aligned} \tag{6.42}$$

where the ξ_n are the positive roots of $\xi_n tan(\xi_n) = \bar{\rho}a/D$.

(b) Cylindrical geometry (bounded by $r = a$)

$$\begin{aligned} I_n &= \frac{4J_1^2(\xi_n)}{\xi_n^2[J_0^2(\xi_n) + J_1^2(\xi_n)]} \\ T_n &= \frac{a^2}{D\xi_n^2} \end{aligned} \tag{6.43}$$

where the ξ_n are the positive roots of $\xi_n J_1(\xi_n)/J_0(\xi_n) = \bar{\rho}a/D$.

(c) Spherical geometry (bounded by $r = a$)

$$\begin{aligned} I_n &= \frac{12[sin(\xi_n) - \xi_n cos(\xi_n)]^2}{\xi_n^2[2\xi_n - sin(2\xi_n)]} \\ T_n &= \frac{a^2}{D\xi_n^2} \end{aligned} \tag{6.44}$$

where the ξ_n are the positive roots of $1 - \xi_n cot(\xi_n) = \bar{\rho}a/D$.

Figure 6.7 shows the dependence of the mode amplitudes on the parameter $\bar{\rho}a/D$. The fast-exchange limit corresponds to $\bar{\rho}a/D \ll 1$. Here the relaxation is single mode,

[3]In their original paper, Brownstein and Tarr formulate the rectangular geometry with only one planar surface 'active'. Hence their definition of the boundaries as being $z = 0$ to $z = a$.

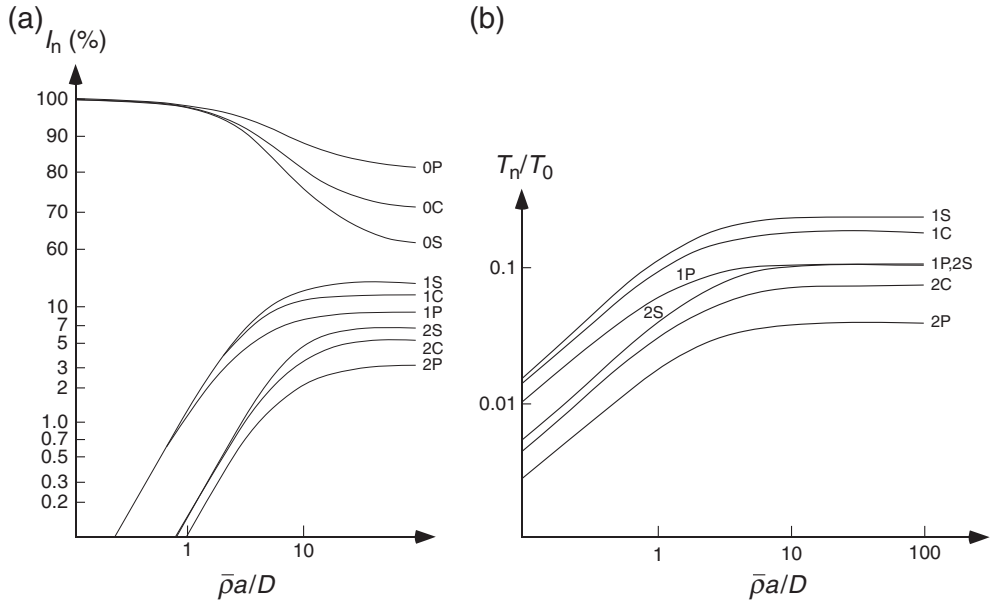

Fig. 6.7 (a) Relative amplitude (I_n) of the nth mode as a function of the dimensionless sink parameter, $\bar{\rho}a/D$, for three geometries: planar (nP), cylindrical (nC), and spherical (nS). (b) Corresponding relaxation times of different modes, normalised to T_0. (Adapted from K. R. Brownstein and C. E. Tarr [35]).

dominated by the slowest relaxation rate, $T_0^{-1} \sim \bar{\rho}(S/V)$, where S/V is the pore surface-to-volume ratio.

The intermediate ($\bar{\rho}a/D \sim 1$) and slow ($\bar{\rho}a/D \gg 1$) regimes feature multi-exponential relaxation, although in the former case the decay is overwhelmingly dominated by the lowest mode. The slow regime is characterised by $\xi_0 \sim 1$ (for example $\xi_0 = \pi$ for the spherical case). Hence $T_0 \sim a^2/D$ for $\bar{\rho}a/D \gg 1$. The physical interpretation is that the relaxation time corresponds to the time taken to migrate across the pore, each spin that hits the wall being lost to relaxation in this slow limit.

Examination of eqns 6.42, 6.43, and 6.44 shows that in the slow regime, the higher mode decay rates, T_n^{-1}, are almost independent of $\bar{\rho}$ and of order $a^2/n^2\pi^2 D$. This is helpful because it gives us an estimate of the range of pore sizes that can be probed. Relaxation times can be measured in the range 1 ms to 2 s leading to a size range of 1–30 μm. Unfortunately, the higher modes represent a small faction of the total signal and are difficult to identify independently. Because of the initial slope is also sensitive to the mode amplitudes, it depends strongly on $\bar{\rho}$. In slow and intermediate regimes both the initial decay rate, T_i^{-1}, and the ratio of T_i to the longest relaxation time, T_0, have characteristic values,

$$T_i^{-1} = \bar{\rho}\frac{S}{V} \tag{6.45}$$

Table 6.1 Dominant mode relaxation times in the fast-diffusion and diffusion-limited regimes according to the Brownstein-Tarr model

	Fast-diffusion $(\bar{\rho}a/D) \ll 1$	Diffusion-limited $(\bar{\rho}a/D) \gg 1$
T_0	$a/\bar{\rho}$	a^2/D

and

$$\frac{T_0}{T_i} = \alpha \frac{\bar{\rho}a}{D} \tag{6.46}$$

where α is, respectively, 0.41, 0.35, and 0.31 for the three geometries considered. The second relation is helpful in estimating the dimensionless parameter $\bar{\rho}a/D$ from the ratio T_i/T_0.

Despite the difficulty in obtaining reliable independent estimates for $\bar{\rho}$, the Brownstein–Tarr model has been widely and successfully used to obtain pore-size distributions from multi-exponential relaxation data [37–39]. In this respect it provides a useful complement to q-space imaging. Conversely, the Brownstein–Tarr model tells us how the PGSE components will be weighted according to local geometry. Because PGSE NMR will tend to emphasise the longest relaxation time components, the behaviour of the dominant $n = 0$ term is of interest. Since V/S is of order a, T_0 is given to within a factor of order unity by Table 6.1.

In discussing the problem of diffusion in fractal volumes, we noted that surface sink relaxation could provide a dimensional measure in the case of surface fractal behaviour. This problem has been treated by de Gennes [40] in the diffusion-limited regime.

6.4 Diffusion in local inhomogeneous fields

Heterogeneous media, when placed in a the polarising magnetic field of an NMR apparatus, will exhibit local spatial variations in field due to susceptibility inhomogeneity. We will label these local fields $\Delta\mathbf{B}_0(\mathbf{r})$, and note that they are superposed on the polarising field $B_0\hat{\mathbf{k}}$. For the molecules of a liquid occupying the pore space of such a medium, the field variations result in differential Larmor precession and hence a phase-spreading, which is manifest as an NMR signal attenuation. Unlike the Brownstein–Tarr (surface-sink) relaxation process associated with wall collisions, relaxation due to susceptibility inhomogeneity arises from through-space interactions that are modulated as the molecule diffuses. Whether surface-sink or susceptibility-inhomogeneity effects are more important will depend on the particular material being studied.

We have seen that the Brownstein–Tarr model leads to a specific signature in the form of the relaxation normal modes. Furthermore the surface-sink mechanism influences both T_1 and T_2 relaxation. In this respect relaxation due to susceptibility effects is quite different. T_1 relaxation requires spin Hamiltonian fluctuations at the Larmor frequency. The spin Zeeman interactions due to susceptibility variations in the sample modulate much more slowly than the Larmor frequency as the particle diffuses and so influence T_2 alone. The existence of susceptibility effects is therefore indicated

by $T_2 \ll T_1$. One nice feature of this difference is that we are able to separate the influences of surface-sink and susceptibility-variation effects by separately observing T_1 and T_2.

6.4.1 Calculating the local field

In a porous medium, typical diamagnetic susceptibility variations, $\Delta\chi$, are on the order 10^{-6}, leading to local magnetic field variations, $\Delta B \sim \chi B_0$, on the order of a few parts per million of the polarising field. This fact greatly simplifies the calculation of local fields, $\mathbf{\Delta B}(\mathbf{r})$, since the local magnetisation induced by the field is dominated by B_0 alone, allowing a simple linear superposition of fields calculated by summing local magnetisation components. In particular, in a region of the material where the diamagnetic susceptibility is $\chi(\mathbf{r})$, the local magnetisation is

$$\mathbf{M}(\mathbf{r}) = \frac{1}{\mu_0}\chi(\mathbf{r})B_0\hat{\mathbf{k}} \tag{6.47}$$

with the local magnetic dipole moment associated with an element of volume dV being $\mathbf{M}(\mathbf{r})dV$. In consequence, the local field offset at any position $\mathbf{r}'$ is simply given by the dipolar field superposition

$$\mathbf{\Delta B}(\mathbf{r}') = \frac{\mu_0}{4\pi}\int_V \Big[3\frac{\mathbf{M}(\mathbf{r})\cdot(\mathbf{r}'-\mathbf{r})}{|\mathbf{r}'-\mathbf{r}|^5}(\mathbf{r}'-\mathbf{r}) - \frac{\mathbf{M}(\mathbf{r})}{|\mathbf{r}'-\mathbf{r}|^3}\Big]d\mathbf{r} \tag{6.48}$$

The summation process is illustrated in Fig. 6.8, for a simple two-phase medium consisting of a solid with susceptibility χ_1 and a liquid with susceptibility χ_2.

Because the magnitude of local field variations, $|\mathbf{\Delta B}(\mathbf{r})|$, are significantly smaller than the magnitude of the polarising field, B_0, from an NMR perspective we need only consider components of that local field parallel to the polarising field. $\mathbf{\Delta B}(\mathbf{r})\cdot\hat{\mathbf{k}}$ will henceforth be labelled $\Delta B(\mathbf{r})$.

A particularly simple example of a porous medium is that of a random monodisperse sphere pack. In this case each sphere generates a local field beyond its boundary equivalent to that of a dipole placed at the sphere centre. Thus the field in the liquid may be obtained by simply summing the contributions from each sphere. An example of the resulting local field map is shown in Fig. 6.9.

6.4.2 Effect of molecular diffusion and the Anderson–Weiss treatment

Of course, spin translational motion will cause the local field to fluctuate. In analogy with the Eulerian velocity field, $\mathbf{v}(\mathbf{r})$, and the Lagrangian distribution of time-dependent velocities, $\mathbf{v}(t)$, we could define, for the spin ensemble, a distribution of fluctuating fields $\Delta B(t)$ and associated Larmor frequencies, $\Delta\omega_0(t)$. The crucial factor in determining the effect on the transverse magnetisation is the rate at which this frequency fluctuates. This rate is characterised by defining the correlation time,

$$\tau_c = \int_0^\infty \frac{\langle\Delta\omega_0(t+\tau)\Delta\omega_0(t)\rangle}{\langle\Delta\omega_0^2\rangle}d\tau \tag{6.49}$$

where $\langle\Delta\omega_0^2\rangle$ is the mean-square frequency fluctuation. $\langle\Delta\omega_0^2\rangle$ is the second moment (M_2) of the linewidth that prevails in the case of a stationary interaction

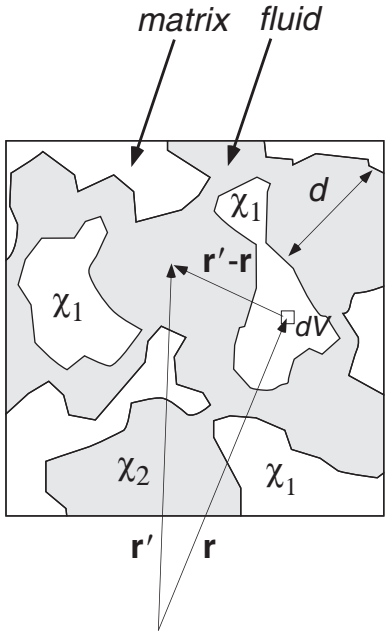

Fig. 6.8 Geometry of local field integration associated with eqn 6.48.

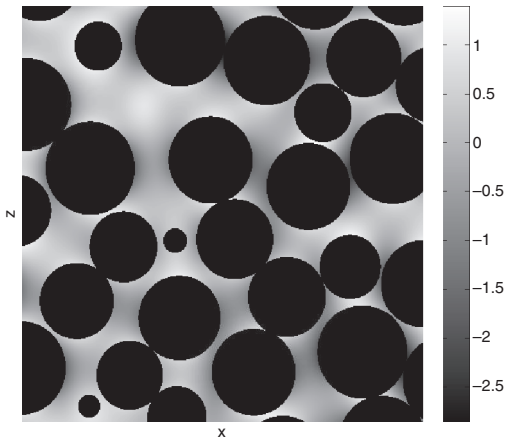

Fig. 6.9 Simulated internal magnetic field (in dimensionless units) for a slice through a sphere pack in which the diamagnetic susceptibility of the spheres and surrounding fluid differ. (Reproduced with permission from Burcaw *et al.* [41].)

($\tau_c \to \infty$) . τ_c depends on the molecular motion and on the correlation length of the field offset, $\Delta\omega_0(\mathbf{r})$. For the moment we ignore these details. We can therefore define 'rapid fluctuations' and 'slow fluctuations' according to $\tau_c^{-1} \gg (\langle\Delta\omega_0^2\rangle)^{1/2}$ or $\tau_c^{-1} \ll (\langle\Delta\omega_0^2\rangle)^{1/2}$, respectively.

The effect of fluctuating local fields on the nuclear transverse magnetisation is well known and has been treated in detail by Abragam [42]; the application of this theory to relaxation induced by diffusion in a spatially varying local field has been made by Packer [43] and Hazelwood *et al.* [44]. Slow fluctuations result in inhomogeneous line broadening. This means that the differing local fields cause differing local precession rates, thus leading to a decay of the transverse magnetisation of the form $\exp(-\frac{1}{2}M_2t^2)$. The essential feature of inhomogeneous broadening is that this decay can be refocused in a spin echo. By contrast, rapid fluctuations result in homogeneous broadening, a true relaxation mechanism common to all spins in the system. Decay due to homogeneous broadening is irreversible because of its stochastic nature. For rapid fluctuations this relaxation is described by a T_2 value of $(M_2\tau_c)^{-1}$.

The general behaviour of both the spin-echo signal and the transverse magnetisation can be treated at any timescale using the Anderson–Weiss theory and the fluctuating field correlation function,

$$g_\omega(\tau) = \frac{\langle \Delta\omega_0(t+\tau)\Delta\omega_0(t)\rangle}{\langle \Delta\omega_0^2\rangle} \tag{6.50}$$

From the assumption that the distribution of $\Delta\omega_0$ is Gaussian, it may be shown that the normalised FID signal, $S(t)$,[4] and the normalised Hahn echo amplitude, $E(2\tau)$, are given respectively by

$$\begin{aligned} S(t) &= \exp(-\langle\Delta\omega_0^2\rangle \int_0^t (t-t')g_\omega(t')dt') \\ E(2\tau) &= \exp(-\langle\omega_0^2\rangle\{4\int_0^\tau (\tau-t')g_\omega(t')dt' - \int_0^{2\tau}(2\tau-t')g_\omega(t')dt'\}) \end{aligned} \tag{6.51}$$

For stochastic processes it is common to assume a correlation function $g_\omega(\tau) = exp(-|\tau|/\tau_c)$. This leads to

$$\begin{aligned} S(t) &= \exp(-\langle\Delta\omega_0^2\rangle\tau_c^2\{\exp(-t/\tau_c) - 1 + t/\tau_c\}) \\ E(2\tau) &= \exp(-\langle\omega_0^2\rangle\tau_c^2\{4\exp(-\tau/\tau_c) - \exp(-2\tau/\tau_c) + 2\tau/\tau_c - 3\}) \end{aligned} \tag{6.52}$$

Figure 6.10 shows the transition from slow to fast regimes in the decay of the FID and spin echo, as represented by eqns 6.52. Although the concept of a relaxation time can only be defined precisely in the fast limit, it is convenient to use the symbols T_2^* and $T_2^\dagger$ to represent the time taken for the FID and echo amplitudes to decay to e^{-1}.

In Chapter 5 we dealt with the problem of diffusion in a steady, uniform, field gradient and generated an expression for magnetisation decay which depended exponentially on the square of the gradient. This expression is not generally applicable in the case of a randomly varying field offset. This can be immediately recognised by

[4]Here we mean the signal $M(t)$ normalised to its initial value $M(0)$.

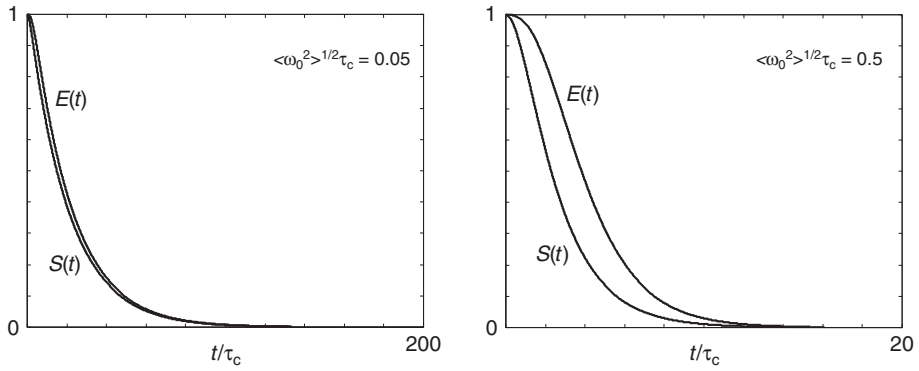

Fig. 6.10 Dependence of FID ($S(t)$) and echo amplitude ($E(t) = E(2\tau)$) on time t for (left) fast motion, where $\langle\Delta\omega_0^2\rangle\tau_c^2 = 0.05$ and (right) intermediate motion, where $\langle\Delta\omega_0^2\rangle\tau_c^2 = 0.5$. Note that $S(t)$ and $E(t)$ converge to a common exponential decay in the fast-motion limit, where relaxation effects dominate.

considering the spin phase, $\int \gamma\Delta B dt$. In the uniform gradient there is no upper bound on the phase as the particle diffuses, since $\Delta B = \mathbf{G}\cdot\mathbf{r}$ and $\mathbf{r}$ is unbounded. This means that the process can be viewed as an unrestricted random phase walk. In the case of the fluctuating local field offset, there is clearly an upper bound on ΔB, which oscillates about 0. To this extent the latter process may be viewed as a restricted phase walk, and the treatment required is quite different.

However the echo expression in eqn 6.52 does have a correspondence with the steady gradient expression for echo attenuation, provided that the diffusion time τ is much shorter than that required to diffuse a characteristic length l_c of the fluctuating field. In the limit $\tau \ll \tau_c$ eqn 6.52 becomes

$$\begin{aligned} E(2\tau) &= \exp(-\tfrac{2}{3}\langle\omega_0^2\rangle\tau_c^{-1}\tau^3) \\ &\approx \exp(-\tfrac{2}{3}\gamma^2\langle G_0^2\rangle D\tau^3) \end{aligned} \tag{6.53}$$

where $\gamma^2\langle G_0^2\rangle = \langle\omega_0^2\rangle/l_c^2$ and we have set $l_c^2 \approx D\tau_c$. The resemblance to eqn 5.45, is obvious.

6.4.3 Measuring relaxation in porous media.

NMR spin relaxation is used extensively in petrophysical applications to measure porosity, pore size distributions, and even permeability. In porous rocks of petrophysical interest, pore sizes range from sub-micron to millimetre. However it is the small pores that provide the dominant interest, since these determine the permeability of the rock and the degree to which ingressed hydrocarbon can be extracted. For such pores, on the order of 10-micron size or smaller, the fast diffusion limit applies and so T_1 and T_2 may be directly related to the pore surface-to-volume ratio. For water in large pores, bulk relaxation behaviour dominates, and from a practical perspective one may write the summed effect as

$$\frac{1}{T_2} = \frac{1}{T_{2bulk}} + \bar{\rho}_2 \frac{S}{V} + \frac{\gamma^2 \langle G_0^2 \rangle D(2\tau)^2}{12}$$
$$\frac{1}{T_1} = \frac{1}{T_{1bulk}} + \bar{\rho}_1 \frac{S}{V} \tag{6.54}$$

where $\bar{\rho}_2$ and $\bar{\rho}_1$ are, respectively, the surface relaxivities for T_2 and T_1 relaxation and the diffusion term in the T_2 expression allows for attenuation due to local inhomogeneous fields, and may be rendered insignificant by choosing the echo time $TE = 2\tau$ sufficiently short.

The distribution of pore sizes leads to a distribution in relaxation rates. Multi-exponential relaxation data may be inverted to yield relaxation-time distributions, using the inverse Laplace technique described in Chapter 9. Of course, converting a distribution of T_2 into a pore-size distribution requires some knowledge of $\bar{\rho}_2$, a parameter which will vary depending on the nature of the rock formation. However, other laboratory methods, such as mercury porosimetry, can be used for calibration purposes, thus enabling petroleum engineers to interpret NMR logging data obtained using tools that are lowered down the well at the drill site.

There exists a considerable body of engineering experience in interpreting NMR relaxation data obtained in this manner. However, amongst the most useful concepts is the idea of a 'T_2 cutoff'. This limit corresponds to pore sizes for which water cannot be removed from the rock by centrifugation, the so-called BVI or 'bulk volume irreducible' by which this bound water is labelled. Not only does the cutoff value give some idea of the degree to which fluid may be extracted from the rock, separating as it does the BVI and FFI (free fluid) fractions, when combined with a knowledge of the porosity, it is also an important parameter in helping estimate rock permeability [45]. Total porous medium porosity can be measured by NMR, comparing the initial, unrelaxed signal intensity (extrapolated from a CPMG train) of a water-saturated sample and a bulk water sample of the same volume. The cutoff is determined by carrying out T_2 distribution measurements in both a fully water-saturated sample and in the same sample after centrifugation has removed all but the irreducible water. The point where the cumulative distributions for the saturated and irreducible water samples separate defines the cutoff [45]. A schematic illustrating these ideas is shown in Fig. 6.11.

6.4.4 Decay due to diffusion in the internal field

The discussion of the previous section concerns the effect of molecular migration in the inhomogeneous field in the case of two canonical NMR measurements, the FID following a 90° RF pulse, and the $90° - 180°-$ spin echo. In both cases T_2 relaxation associated with surface collisions causes additional attenuation. By clever design of the NMR pulse sequence, it is possible to access field migration and relaxation effects separately. One such method is the DDIF (decay due to diffusion in the internal field) experiment of Song *et al.* [46]. The RF pulse sequence is shown in Fig. 6.12. t_e is chosen sufficiently short ($t_e \ll \tau_c$) that the molecules diffuse shorter distances than the characteristic length, $\sqrt{2D\tau_c}$, over which variation occurs in the local field, $\Delta B(\mathbf{r})$. By contrast, t_d is sufficiently long that diffusion results in significant changes in $\Delta B(\mathbf{r})$. Of course, there will be a decay caused by T_1 relaxation over the time t_d. This may

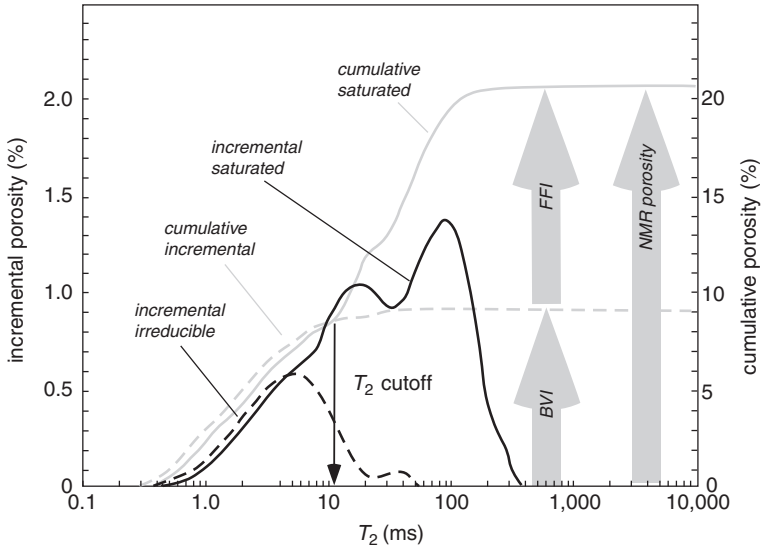

Fig. 6.11 Schematic NMR determination of T_2 cutoff in a porous rock. The solid data lines of the incremental and cumulative T_2 distributions refer to a fully water-saturated rock sample while the dashed data lines refer to measurements in a rock that has been centrifuged to leave only the irreducible water. (Adapted from Coates *et al.* [45])

be removed by normalising the echo signal, $E(t_e, t_d)$, by the reference signal, $R(t_e, t_d)$, obtained using pulse sequence (b) in Fig. 6.12. With this step one obtains the DDIF signal

$$E_n(t_e, t_d) = \int\int \rho(\mathbf{r}) e^{i\gamma t_e(\Delta B(\mathbf{r}) - \Delta B(\mathbf{r}'))} P(\mathbf{r}|\mathbf{r}', t_d) d\mathbf{r} d\mathbf{r}' \tag{6.55}$$

where the signal is taken to be 'on-resonance', so that the precession due to the polarising field, B_0, is neglected.

The decay represented by eqn 6.55 is rather similar to that resulting from molecular diffusion in a steady gradient, but with one major difference: unlike the case for steady gradients, $B_0(\mathbf{r})$ is bounded with the full range of values sampled over the pore length scale. At short times t_d, $E_n(t_e, t_d)$ decays approximately as $1 - \frac{1}{2}\gamma^2 t_e^2 \langle(\Delta B(\mathbf{r}) - \Delta B(\mathbf{r}'))^2\rangle$, the term in the angular brackets increasing with increasing t_d. But because of the normalisation with $R(t_e, t_d)$, the DDIF signal reaches an asymptotic value for large t_d, as $\Delta B(\mathbf{r}')$ and $\Delta B_0(\mathbf{r})$ become uncorrelated. Expressing the DDIF signal in terms of the distribution of local fields, $f(\Delta B)$,

$$E_n(t_e, t_d) = \int_{\Delta B_{min}}^{\Delta B_{max}} \int_{\Delta B_{min}}^{\Delta B_{max}} f(\Delta B) e^{i\gamma t_e(\Delta B - \Delta B')} P(\Delta B|\Delta B', t_d) d\Delta B d\Delta B' \tag{6.56}$$

For $t_c \gg \tau_c$, the conditional probability $P(\Delta B|\Delta B', t_d)$ is independent of starting field and reduces to $f(\Delta B')$. Whence

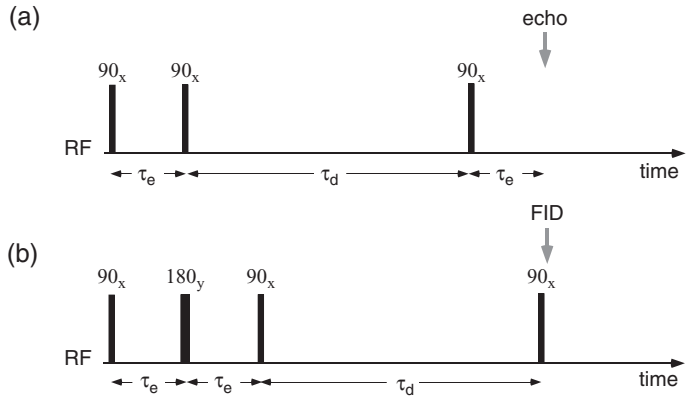

Fig. 6.12 Pulse sequences used for the DDIF method. (a) Encoding due to dephasing in the the local field over two periods t_e separated by t_d. (b) Encoding for T_1 relaxation while dephasing in the local field is cancelled by the spin echo.

$$E_n(t_e, t_d \to \infty) = |\int_{\Delta B_{min}}^{\Delta B_{max}} f(\Delta B) e^{i\gamma t_e \Delta B} d\Delta B|^2$$
$$= |S(t_e)|^2 \tag{6.57}$$

where $S(t)$ is the (relaxation-normalised) FID.

Figure 6.13 shows an example of the DDIF signal obtained from water diffusing in a random glass sphere pack.

The rate of the DDIF decay is determined by the characteristic length, $l_c = \sqrt{2D\tau_c}$, over which the local field fluctuations are manifest. Clearly, this length will depend upon pore size, so that a multi-exponential analysis of the decay can yield a pore-size distribution, much in the same way that multiexponential analysis of relaxation times is used in porous media.

6.4.5 q-space analysis of internal field correlations

Equation 6.55 demonstrates the role of the displacement propagator in governing the effects of diffusion in the inhomogeneous field within a porous medium. Access to that propagator is provided in natural manner by the use of pulsed magnetic field gradients. Cho and Song [47] have suggested a clever PGSE NMR approach for examining magnetic field correlations for liquid molecules diffusing in porous media. The method depends on the use of two pulsed gradient sequences, one in which internal field effects are cancelled out and another in which they induce phase shifts. In both sequences relaxation due to T_1 and T_2 plays an identical role, so that by taking a ratio of the signals from each experiment, relaxation effects can be revealed.

The two sequences, which each generate stimulated echoes, are shown in Fig. 6.14. In the first of these (a), the 180° RF pulses refocus the effect of dephasing in the local field $\Delta B(\mathbf{r})$, while the gradient pulses produce an encoding for displacement over the time period of approximately τ_d. Note that the sequence shown effectively consists of a single effective gradient pair, each gradient pulse being split around the 180° RF pulse

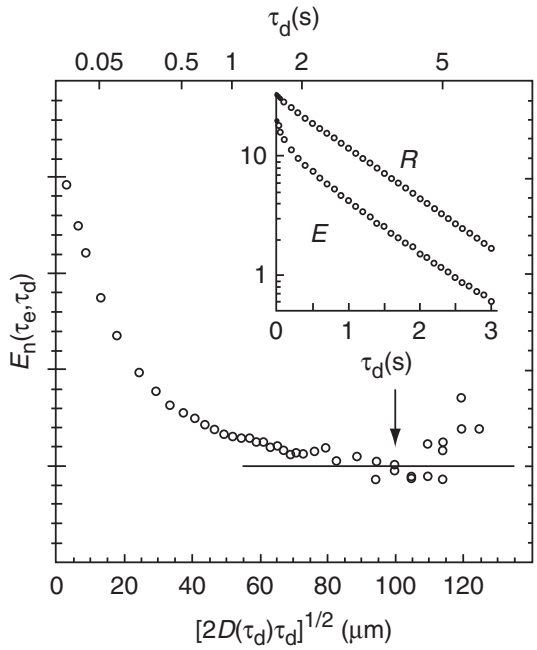

Fig. 6.13 DDIF ratio (E/R) for water diffusing in a uniform-size, randomly packed 100-micron diameter glass bead sample. The ratio is shown as a function of the rms displacement,$(2D(t_d)t_d)^{1/2}$, with the corresponding t_d shown at the top of the graph. The line is the square of the FID. (Figure adapted from Song *et al.* [46].)

with opposite sign in the dephasing and rephasing periods τ_e, so that each contributes the same sign effective gradient to the $q-$encoding, along the lines of the 13-interval Cotts sequence. For this sequence the signal is

$$\begin{aligned} E(\mathbf{q},\tau_d) &= \int \rho(\mathbf{r})P(\mathbf{r}|\mathbf{r}+\mathbf{R},\tau_d)e^{i\mathbf{q}\cdot\mathbf{R}}d\mathbf{r}d\mathbf{R} \\ &= \int \bar{P}(\mathbf{R},\tau_d)e^{i\mathbf{q}\cdot\mathbf{R}}d\mathbf{R} \end{aligned} \tag{6.58}$$

In the second sequence, (b), the positions of the 180° RF pulses are shifted so that the dephasing (τ_e) and rephasing (τ_e') periods are unequal, leading to additional phase shifts due to the local fields, and the result

$$\begin{aligned} E(\mathbf{q},\tau_d) &= \int \rho(\mathbf{r})P(\mathbf{r}|\mathbf{r}+\mathbf{R},\tau_d)e^{i\mathbf{q}\cdot\mathbf{R}}e^{it\gamma(\Delta B(\mathbf{r})-\Delta B(\mathbf{r}+\mathbf{R}))}d\mathbf{r}d\mathbf{R} \\ &= \int \bar{P}(\mathbf{R},\tau_d)e^{i\mathbf{q}\cdot\mathbf{R}}\langle e^{it\gamma(\Delta B(\mathbf{r})-\Delta B(\mathbf{r}+\mathbf{R}))}\rangle d\mathbf{R} \end{aligned} \tag{6.59}$$

where $t=\tau'-\tau$, and where $\langle\ldots.\rangle$ in eqn 6.59 represents an average over all starting positions $\mathbf{r}$. Taking the Fourier transform with respect to $\mathbf{q}$ of eqns 6.58 and 6.59 gives the probabilities $\bar{P}(\mathbf{R},\tau_d)$ and $\bar{P}'(\mathbf{R},\tau_d)$, respectively, such that

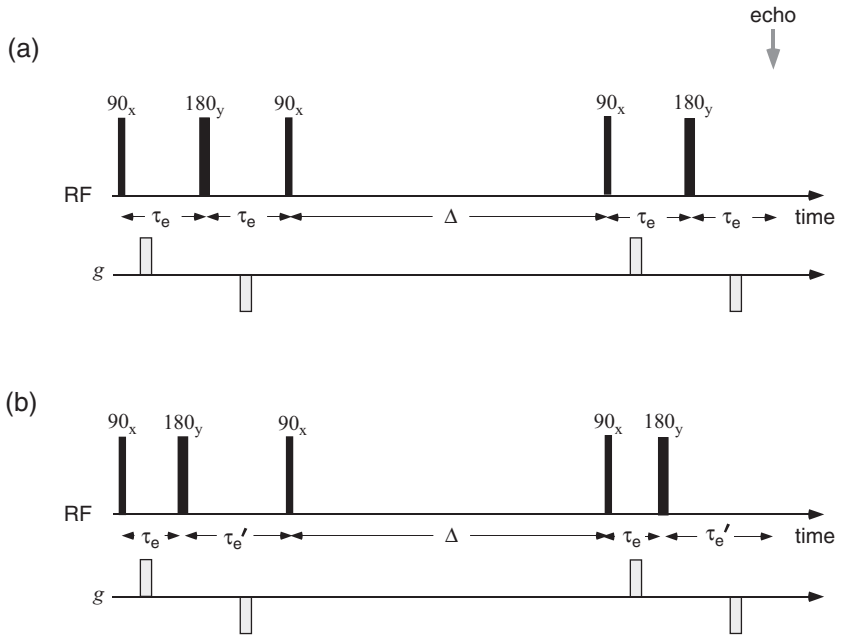

Fig. 6.14 Pulse sequence used by Cho and Song [47] to measure pair correlation function of internal magnetic field: (a) balanced sequence and (b) imbalanced sequence.

$$\begin{aligned}\bar{P}'/\bar{P} &= \langle e^{it\gamma(\Delta B(\mathbf{r})-\Delta B(\mathbf{r}+\mathbf{R}))}\rangle \\ &\approx 1-\gamma^2t^2\langle\Delta B^2\rangle+\gamma^2t^2\langle\Delta B(0)\Delta B(\mathbf{R})\rangle \end{aligned} \tag{6.60}$$

where $\langle\Delta B(0)\Delta B(\mathbf{R})\rangle$ is the inhomogeneous field pair correlation function, and $\langle\Delta B^2\rangle$ is the second moment of the field, easily obtained by examination of the NMR linewidth. Note that the role of τ_d is simply to determine the sensitivity of the signal to the full range of displacements $\mathbf{R}$. Reference [47] contains a number of examples of pair correlation function measurements for water diffusing in glass beadpacks.

6.5 Restricted diffusion for spin echoes with steady gradients

Section 6.2 dealt with the effect of boundaries and restrictions on diffusion. Sections 6.3 and 6.4 outlined the influence on spin relaxation of molecular motion in heterogeneous structures, both from the standpoint of exchange between regions of differing local relaxation rates, and where structural heterogeneities result in locally inhomogeneous magnetic fields. The remaining sections of this chapter deal with the influence of restricted motion on spin-echo NMR experiments in which external gradients are deliberately applied.

We begin by considering the steady gradient spin echo, in part because of its historical interest, but also because it provides a limiting case for the PGSE experiment and

one with considerable practical application. In early papers, Robertson [48] and Neuman [49] addressed the problem of the steady gradient spin-echo decay in a bounded region, in both cases utilising the Gaussian phase approximation in order to obtain closed-form expressions for spin echo amplitudes. Before examining examples for specific geometries based on their ideas, it is helpful to outline a more general physical picture of relevant motional regimes.

6.5.1 Characteristic length scales

The most obvious characteristic length scale is the distance diffused by molecules over a given time τ. The diffusion length, l_D, is defined by

$$l_D = (D_0\tau)^{1/2} \tag{6.61}$$

The second length scale is that associated with dephasing in the magnetic field gradient. Equation 5.42 tells us that the mean-squared phase shift experienced by an ensemble of spins borne by molecules in free diffusion, in the presence of a constant magnetic field gradient g, and after a diffusion time τ, is given by

$$\begin{aligned}\langle\phi^2\rangle &= \tfrac{1}{3}\gamma^2 g^2 \tau_s^2 \xi^2 n^3 \\ &= \tfrac{1}{3}\gamma^2 g^2 D_0 \tau^3\end{aligned} \tag{6.62}$$

Note that the accumulation of phase depends in part on the mean-squared displacement $n\xi^2$, but also on the residence time per step, during which a phase $\gamma g \tau_s$ is acquired. This means that the more rapid the diffusion, the greater rms distance a spin-bearing molecule must diffuse in order to acquire a given rms phase shift. This idea is neatly encapsulated by defining a 'dephasing length' [50]

$$l_g = \left(\frac{D_0}{\gamma g}\right)^{1/3} \tag{6.63}$$

l_g is a measure of the molecular diffusion distance corresponding to a spin phase shift on the order of 2π. Note that l_g is related to both the gradient amplitude and the rate of diffusion, but is independent of the diffusion time τ. One gradient-related length scale that does depend on τ is the magnetisation helix wavelength,

$$\lambda = \frac{2\pi}{\gamma g \tau} \tag{6.64}$$

The length scales l_D, l_g, and λ are interdependent since $l_g = (\lambda l_D^2/2\pi)^{1/3}$. Together, eqns 6.63, 6.61, and 6.64 tell us that the echo attenuation for free diffusion in the presence of a steady gradient at echo time 2τ, may be written [51]

$$\begin{aligned}E &= \exp(-\tfrac{2}{3}\gamma^2 g^2 D_0 \tau^3) \\ &= \exp\left(-\frac{2}{3}\left[\frac{l_D}{l_g}\right]^6\right) \\ &= \exp\left(-\frac{2}{3}4\pi^2\left[\frac{l_D}{\lambda}\right]^2\right)\end{aligned} \tag{6.65}$$

Finally, when dealing with restricted diffusion, another length scale emerges, the characteristic distance between boundaries, l_s [51]. This is the distance a molecule may freely diffuse before encountering restrictions to its Brownian motion. Note that for the case of free diffusion, as $l_D \gg l_g$, the echo signal disappears. However, in the case of restricted motion, very different behaviours are apparent, according to the relative sizes of l_D, l_g, and l_s.

6.5.2 Regimes of interest

Figure 6.15 shows a fluid bounded by plane slabs in which molecular diffusion is depicted under a range of comparative length scales. Neglecting the effect of gradients, we can clearly distinguish the diffusive behaviour in the cases $l_D \ll l_s$ and $l_D \gg l_s$. In the former, the diffusion is largely free apart from a small proportion of molecules experiencing wall collisions, the impact on the apparent diffusion coefficient having been discussed in Section 6.1.2. In the latter case the apparent diffusion coefficient reduces asymptotically to zero, while the mean-squared displacement becomes fixed and on the order of l_s^2. However, in a steady gradient spin-echo experiment the behaviour is more subtle, as the length scale associated with dephasing in the gradient starts to play a role. Hürlimann *et al.* [51] have identified three regimes where differing behaviours dominate. While these can be characterised by using the set (l_D, l_s, λ), a better parametrisation is provided by the set (l_D, l_s, l_g).

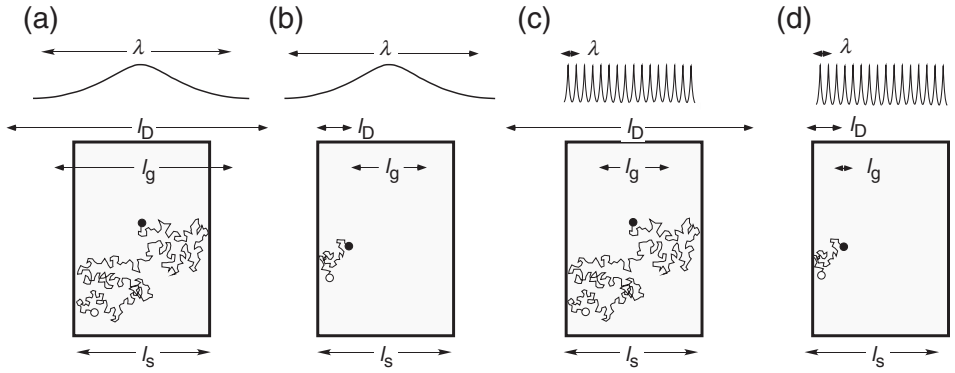

Fig. 6.15 Characteristic length scales for molecules diffusing between two plane parallel slabs, and with the magnetic field gradient applied normal to the planes: (a) corresponds to the motional averaging regime, (b) to the free-diffusion regime, while (c) and (d) correspond to the localisation regime.

Free diffusion regime: $l_D/l_s \ll 1$ and $l_D/l_g \ll 1$ (l_D shortest length)
In the free-diffusion regime only a small proportion of molecules collide with the walls and the gradient is sufficiently weak (l_g sufficiently long) that severe echo attenuation does not result. Here one might expect that the free diffusion result holds, but with the apparent diffusion coefficient modified slightly, as outlined in Section 6.1.2, so as to allow for an impeded layer of thickness l_D near the walls. However the precise

expression for the apparent diffusion coefficient that applies in the case of the steady gradient echo under the definition

$$E(g,\tau) = \exp(-\gamma^2 g^2 D_{\text{app}} \tau^3) \tag{6.66}$$

is slightly different from that of eqn 6.14, which is calculated on the basis of the mean-squared displacement. The appropriate expression for D_{app}, which is consistent with eqn 6.66, has been shown by de Swiet and Sen [50] to be

$$D_{\text{app}} \approx D_0(1 - \alpha(S/V)\sqrt{D_0\tau}) \tag{6.67}$$

where $\alpha = 32(2\sqrt{2} - 1)/(105\sqrt{\pi})$. This coefficient is very close to the $4/9\sqrt{\pi}$ that applies in eqn 6.14.

Motional narrowing regime: $l_s/l_D \ll 1$ and $l_g/l_s \gg 1$ (l_s shortest length)
This is the regime analysed by Robertson [48], who found, in the case of restricted diffusion between planar boundaries, the steady gradient echo-attenuation expression

$$\begin{aligned} E(g,\tau) &= \exp\left(-\frac{1}{120}\frac{\gamma^2 g^2 l_s^4 2\tau}{D_0}\right) \\ &= \exp\left(-\frac{1}{60}\left[\frac{l_D}{l_g}\right]^2\left[\frac{l_s}{l_g}\right]^4\right) \end{aligned} \tag{6.68}$$

Note the appearance of the diffusion coefficient in the exponent denominator. For faster diffusion, the phase spreading, and hence the echo attenuation, reduces, and for the simple reason that the molecules are approaching an asymptotic 'averaged' state, in which the molecules appear to reside at their mean position at the box centre between the plane walls. The motional narrowing has occurred because the fluctuation rate for the spin Larmor frequencies exceeds the frequency spread created by the magnetic field gradient across the rectangular pore.

Similar expressions [49] are obtained for different geometries, but with different numerical prefactors in the exponents. Note that these derivations all rely on the use of the Gaussian phase approximation. This approximation becomes questionable when $\gamma^2 g^2 D_0 \tau^3$ is greater than or of order unity, in other words when $l_D \sim l_g$. As we will see in the next section, this breakdown is associated with the appearance of diffraction-like effects in the echo-attenuation function.

Localisation regime: $l_g/l_s \ll 1$ and $l_g/l_D \ll 1$ (l_g shortest length)
This curious regime corresponds to the onset of the edge-enhancement effects seen in Fig. 6.2, where the spins far from the wall have been completely dephased by the gradient pulses and their contribution to the signal disappears. Only spins within a distance l_g of the walls, where restricted diffusion has reduced the spin dephasing effect, contribute significantly to the echo signal [51]. Note that in this regime the phase distribution is not at all Gaussian. This problem in the case of parallel plane boundaries has been addressed in a paper by Stoller *et al.* [52], and again by de Swiet and Sen [50], who find, at long echo times

$$E(g,\tau) = c\frac{D_0^{1/3}}{\gamma^{1/3}g^{1/3}l_s}\exp\left(-a_1\gamma^{2/3}g^{2/3}D_0^{1/3}\tau\right)$$
$$= c\frac{l_g}{l_s}\exp\left(-a_1\left[\frac{l_D}{l_g}\right]^2\right) \tag{6.69}$$

where $a_1 = 1.0188$ and $c = 5.8841$. Note that the exponent, which does not depend on l_s, is expected to apply for all geometries, with only the prefactor c depending on the pore shape.[5]. Experiments in the localisation regime are hard to perform. The

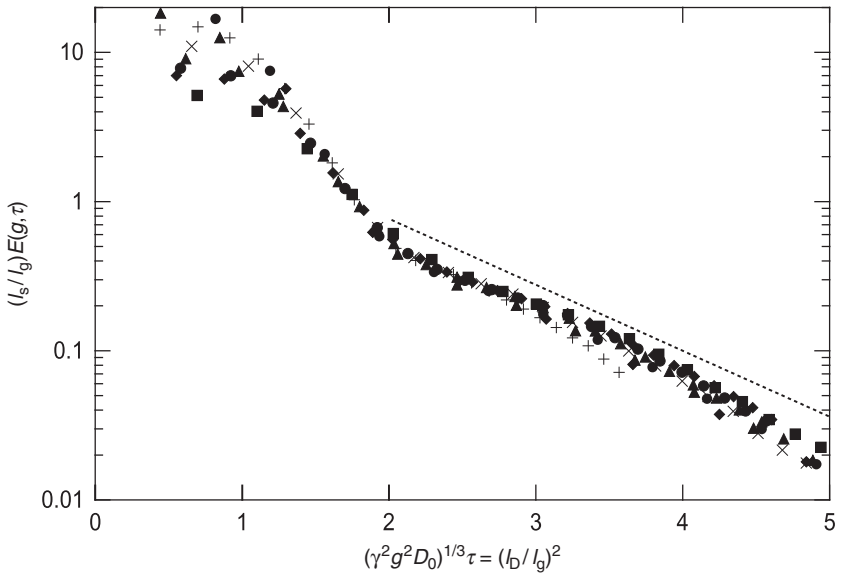

Fig. 6.16 Measured spin-echo amplitude, rescaled according to the predictions of eqn 6.69, as taken from Hürlimann *et al.* [51]. The dashed line corresponds to eqn 6.69.

prefactor l_g/l_s means that signal levels are small and the magnetic field gradients need to be aligned normal to the plane boundaries within a few degrees. However, in a carefully controlled experiment, Hürlimann *et al.* [51] have provided a nice verification of eqn 6.69, as shown in Fig. 6.16.

6.5.3 Alternative non-dimensional parameters

The echo-attenuation expressions for the free diffusion (eqn 6.65), motional narrowing (6.68), and localisation (6.69) regimes can be alternatively expressed in terms of two non-dimensional parameters (p, q) instead of via the three-parameter set (l_D, l_s, l_g). Grebenkov [53] has defined these non-dimensional parameters as[6]

[5] a_1 is the first zero of the derivative of the Airy function $Ai(x)$

[6] Note that q should not be confused with the symbol used for the PGSE wavevector.

$$\begin{aligned} p &= \frac{D_0\tau}{l_s^2} \\ &= \frac{l_D^2}{l_s^2} \end{aligned} \tag{6.70}$$

and

$$\begin{aligned} q &= \gamma g \tau l_s \\ &= \frac{l_D^2 l_s}{l_g^3} \end{aligned} \tag{6.71}$$

whence, eqns 6.65, 6.68, and 6.69 become, respectively,

Free-diffusion regime: $p \ll 1$ **and** $pq^2 \ll 1$

$$E = \exp\left(-\tfrac{2}{3}q^2 p\right) \tag{6.72}$$

Motional-narrowing regime: $p \gg 1$ **and** $p/q \gg 1$
For plane parallel boundaries

$$E = \exp\left(-\tfrac{1}{60}q^2 p^{-1}\right) \tag{6.73}$$

Localisation regime: $p/q \ll 1$ **and** $pq^2 \gg 1$
For plane parallel boundaries at long echo times

$$E = c(p/q)^{1/3} \exp\left(-a_1 (q^2 p)^{1/3}\right) \tag{6.74}$$

The three regimes may be alternatively illustrated in the (q, p) plane [53] or in a plane defined by the ratios $(l_g/l_s, l_D/l_s)$ [51], as shown in Fig. 6.17.

6.6 Pulsed gradient spin-echo NMR for bounded molecules

Section 6.5 dealt with the way in which the confinement of diffusing molecules to a pore or cavity influences the echo attenuation under conditions of a steady magnetic field gradient. In the next chapter we will discover that, when pulsed magnetic field gradients are used, the echo attenuation manifests features akin to that of a diffraction experiment. In the present section, we look beyond restricted diffusion of molecules confined inside a cavity with hard boundaries, and consider environments where spin-bearing molecules or molecular segments exhibit 'softer' restrictions to their motion. For example, a diffusing polymer segment in a cross-linked gel will experience a restoring force due to gel elasticity. This will have the effect of limiting the distribution of translational displacements as Δ becomes large. Another rather unusual form of displacement limitation arises when molecules are confined to diffuse in a curvilinear coordinate system, examples being the motion of solvent molecules along the lamellae in a multi-domain lyotropic liquid crystal or the motion of a random coil polymer molecule in the 'tube' of topological constraints due to neighbouring polymers. In such systems the molecular motion in the laboratory frame exhibits a characteristic dependence on timescale, attenuating as Δ increases. This type of soft bounding might be termed 'dimensionally restricted' diffusion.

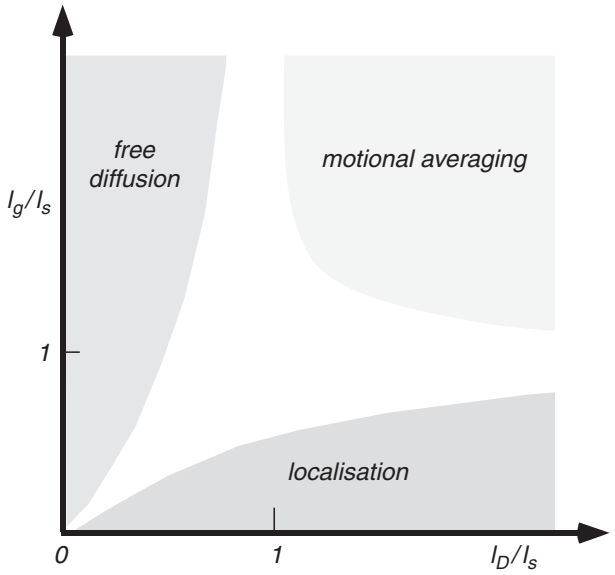

Fig. 6.17 Schematic illustration of the free-diffusion, motional-averaging, and localisation regimes. (Adapted from Hürlimann *et al.* [51].)

6.6.1 Diffusion in a harmonic potential

The problem of diffusion in the presence of an harmonic potential has been considered by Stejskal [54]. In this treatment, the restoring force is balanced by frictional damping due to the viscosity of the surrounding particles. If the ratio of the elastic force constant, k, and the friction coefficient, ζ, is termed β, then the elastic potential is written $V = \frac{1}{2}\beta\zeta\mathbf{r}^2$, with associated force $-\beta\zeta\mathbf{r}$. Equating this with the friction force, $-\zeta\mathbf{v}$, gives $\mathbf{v} = \beta\mathbf{r}$. From eqn 2.53, and treating the diffusion as isotropic with scalar diffusion coefficient D, $P(\mathbf{r}_0|\mathbf{r},t)$ obeys

$$\frac{\partial P}{\partial t} = \beta\nabla\cdot\mathbf{r}P + D\nabla^2 P \tag{6.75}$$

which has the solution

$$\begin{aligned} P(\mathbf{r}_0|\mathbf{r},t) = &\left[2\pi D\left(1-e^{-2\beta t}\right)/\beta\right]^{-3/2} \\ &\times\exp\left[-\frac{\beta\left(\mathbf{r}-\mathbf{r}_0e^{-\beta t}\right)^2}{2D\left(1-e^{-2\beta t}\right)}\right] \end{aligned} \tag{6.76}$$

The equilibrium density can be obtained by using the long-time limit identity of $P(\mathbf{r}_0|\mathbf{r},t)$ and $\rho(\mathbf{r}_0)$, thus

$$\rho(\mathbf{r}_0) = (2\pi D/\beta)^{-3/2}\exp\left(-\beta\mathbf{r}_0^2/2D\right) \tag{6.77}$$

Writing the force constant as $k = \beta\zeta$ and noting that the free particle diffusion coefficient is k_BT/ζ, we can see immediately that eqn 6.79 is the 3-D version of that given in eqn 1.88.

The exponential decay of $\rho(\mathbf{r}_0)$ as the distance from the origin increases is an example of 'soft bounding'. Substitution of $P(\mathbf{r}_0|\mathbf{r},t)$ and $\rho(\mathbf{r}_0)$ into the narrow pulse PGSE expression, eqn 5.78, gives

$$E(\mathbf{q},\Delta) = \exp\left[-4\pi^2 q^2 D\left(1-e^{-\beta\Delta}\right)/\beta\right] \tag{6.78}$$

The dependence of $E(\mathbf{q},\Delta)$ on $\mathbf{q}$ is Gaussian at all timescales. For $\Delta \ll \beta^{-1}$, the behaviour is the same as for unrestricted diffusion. For $\Delta \gg \beta^{-1}$ $E(\mathbf{q},\Delta)$ is independent of Δ and reduces to $|S(\mathbf{q})|^2$, where $S(\mathbf{q})$ is the 1-D Fourier transform of the equilibrium density $\rho(\mathbf{r}_0)$ given in eqn 6.77,

$$E(\mathbf{q},\infty) = \exp(-q^2 D/\beta) \tag{6.79}$$

The PGSE NMR method has been used to study harmonic-well-restricted diffusion for a polymer gel network [55]. The physics of diffusion in polymer gels has been discussed in detail by de Gennes [56]. Given a friction coefficient ϕ per unit volume and bulk modulus E_b, it can be shown that the elastic constant for longitudinal gel fluctuations of wavevector κ is $E_b\kappa^2$ while the cooperative diffusion coefficient, D_c, is $E_b\phi$. For such a system, β is given by [55] $E_b\kappa^2/F_\zeta$.

6.6.2 Diffusion and exchange between two sites

One commonly encountered morphology is one where the diffusional behaviour may be divided into subregions, with molecules confined to an inhomogeneous distribution of local diffusion rates on a short timescale, but where the ensemble of molecules experience all regions over a sufficiently long timescale, so exhibiting a common, averaged diffusion coefficient. The problem of calculating the PGSE NMR signal for molecules in exchange between two regions may be treated in the same manner as for relaxation [57, 58]. Again, in the short-time limit (slow exchange) the echo attenuation consists of a linear superposition from the sub-regions of weighting P_i and local diffusion coefficient D_i,

$$E(g,\Delta) = \exp(-\gamma^2\delta^2 g^2 \bar{D}\Delta) \tag{6.80}$$

Now the coupled differential equations are

$$\frac{dE_{ij}(g,t)}{dt} = -\frac{1}{\tau_j}E_{ij}(t) - \gamma^2\delta^2 g^2 D_j E_{ij}(g,t) + \sum_k E_{ik}(g,t)\frac{1}{\tau_k}p_{kj} \tag{6.81}$$

For a two-phase system [58]

$$\bar{E}(g,\Delta) = a_1\exp(-\gamma^2\delta^2 g^2 D_1'\Delta) - a_2\exp(-\gamma^2\delta^2 g^2 D_2'\Delta)) \tag{6.82}$$

where

$$D_1', D_2' = \frac{1}{2}[D_1 + D_2 + \frac{1}{\gamma^2\delta^2 g^2}(\frac{1}{\tau_1}+\frac{1}{\tau_2}) \tag{6.83}$$

$$\mp\left[\left(D_2 - D_1 + \frac{1}{\gamma^2\delta^2 g^2}(\frac{1}{\tau_2}-\frac{1}{\tau_1})\right)^2 + \frac{4}{\gamma^4\delta^4 g^4\tau_1\tau_2}\right]^{1/2}] \tag{6.84}$$

and

$$a_1 = \frac{1}{D_2' - D_1'}[D_2' - D_{av}]$$
$$a_2 = \frac{1}{D_2' - D_1'}[D_1' - D_{(av)}] \tag{6.85}$$

where

$$D_{av} = P_1 D_1 + P_2 D_2 \tag{6.86}$$

In the long timescale limit these equations reduce, as required, to eqn 6.80 with $\bar{D} = D_{av}$.

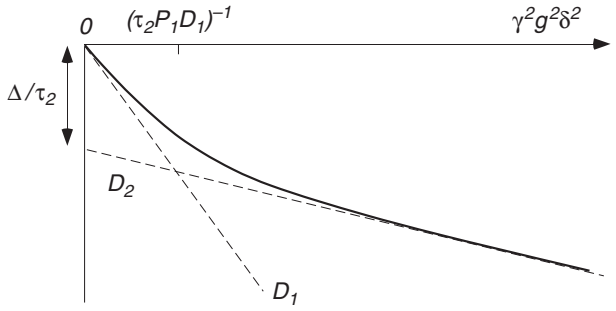

Fig. 6.18 Echo attenuation for two-region diffusion. (Adapted from J. Kärger *et al.* [58].)

One commonly encountered special case concerns the existence of small regions of high mobility ($P_1 \ll P_2$, $D_1 \gg D_2$) for which the echo attenuation simplifies to

$$E(g) = \exp(-\gamma^2 \delta^2 g^2 \left[D_2 + \frac{P_1 D_1}{\gamma^2 \delta^2 g^2 \tau_2 P_1 D_1 + 1} \right] \Delta) \tag{6.87}$$

The exponent term in square brackets represents the effective diffusion coefficient as measured by the PGSE experiment. The limiting slopes and intercepts of the echo-attenuation data allow the determination of D_2, $P_1 D_1$, and τ_2, as illustrated in Fig. 6.18. This approach has been used for describing diffusion in microporous crystallites where the subscripts 1 and 2 refer to the intercrystalline and intracrystalline spaces [59–61].

6.6.3 Dimensional restriction: randomly distributed pipes and sheets

Suppose we try to predict the result of a PGSE NMR experiment in which the molecules have anisotropic diffusion with cylindrical symmetry. In other words, there exists some coordinate frame (x', y', z') in which $D_{x'x'} = D_{y'y'} = D_\perp$, while $D_{z'z'} = D_\parallel$, as shown in Fig. 6.19.

Given that the echo attenuation for spins with a mean-square displacement $\langle Z^2 \rangle$ is $\exp(-\frac{1}{2} q^2 \langle Z^2 \rangle)$, for spins in a region where the axis of symmetry is inclined at polar angle θ to the gradient direction, labelled by z [62]

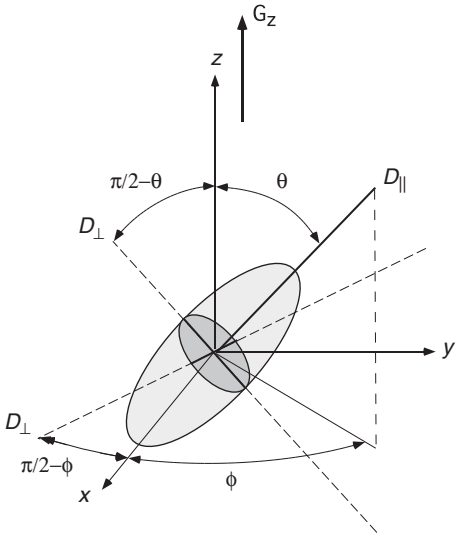

Fig. 6.19 Schematic showing the polar geometry of a randomly oriented locally anisotropic diffusion domain. Cylindrical symmetry is assumed. Two convenient directions in the $D_\perp$ plane are shown, one of which is normal to the z-axis, and the other inclined at $\pi/2 - \theta$.

$$\langle Z^2 \rangle = 2D_\parallel \Delta_r \cos^2\theta + 2D_\perp \Delta_r \sin^2\theta \tag{6.88}$$

where the reduced time has been used in order to give the exact echo-attenuation factor. Hence the net $E(\mathbf{q}, \Delta)$ is the sum obtained by averaging element orientations over all angles, weighted by the sphere area element, $\sin\theta d\theta$. Hence [62]

$$\begin{aligned} E(\mathbf{q}, \Delta_r) &= \int_0^\pi \exp\left[-q^2\Delta_r\left(D_\parallel \cos^2\theta + D_\perp \sin^2\theta\right)\right] \sin\theta d\theta \Big/ \int_0^\pi \sin\theta d\theta \\ &= \exp(-q^2 D_\perp \Delta_r) \int_0^1 \exp\left[-q^2\Delta_r\left(D_\parallel - D_\perp\right)x^2\right] dx \end{aligned} \tag{6.89}$$

Equation 6.89 is very helpful. Suppose that we are dealing with the the problem of water diffusing between the lamellar sheets of a lyotropic liquid crystal. Then the symmetry is 'two-dimensional' or 'lamellar', and $D_\perp \gg D_\parallel$ and, assigning $D_\perp = D$, the echo attenuation varies as

$$E_{2D} = \exp(-q^2 D\Delta_r) \int_0^1 \exp\left[q^2 D\Delta_r x^2\right] dx \tag{6.90}$$

If, on the other hand, the diffusing molecules are confined to narrow pipes, then the symmetry is 'one-dimensional' or 'capillary' and $D_\perp \ll D_\parallel$ with

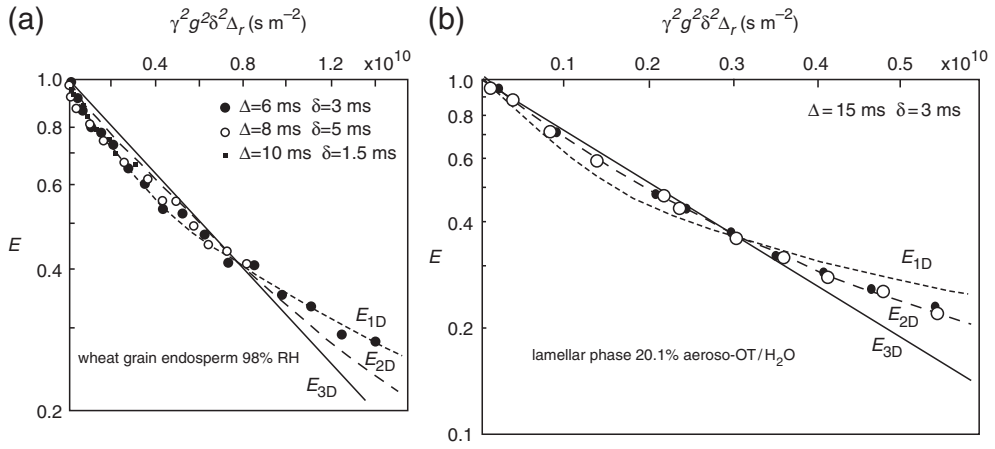

Fig. 6.20 $q^2\Delta_r$-dependence of water proton echo attenuation for (a) wheat grain endosperm tissue equilibrated at 90% relative humidity (RH). The theoretical curves labelled E_{1D}, E_{2D}, and E_{3D} refer to one-, two-, and 3-D diffusion (eqns 6.91, 6.90, and 5.87, respectively) and data obtained at different echo times Δ are consistent with E_{1D}. (Data taken from reference [62].) (b) 20.1% Aerosol OT/water. The data lie on a common curve characteristic of 2-D diffusion, consistent with each molecule residing in a single lamellar domain. Open and closed circles refer to samples after three days and three months' equilibration (Data taken from reference [63].)

$$E_{1D} = \exp(-q^2 D\Delta_r) \int_0^1 \exp\left[q^2 D\Delta_r (1 - x^2)\right] dx$$
$$= \int_0^1 \exp\left[-q^2 D\Delta_r x^2\right] dx \tag{6.91}$$

where in this case we assign $D_\parallel = D$.

Equations 6.90 and 6.91 may be contrasted with the echo attenuation behaviour for unrestricted diffusion, $E_{3D} = \exp(-q^2\Delta_r D)$. The dependence of E_{1D}, E_{2D}, and E_{3D} on $q^2\Delta_r = \gamma^2 g^2 \delta^2 \Delta_r$ gives a characteristic signature in the curvature of the $\log(E(q, \Delta_r))$ vs $\gamma^2 g^2 \delta^2 \Delta_r$. Figure 6.20 shows the echo-attenuation plot for water protons in the polydomain lamellar phase of Aerosol OT/water [63], along with the best fits using E_{1D}, E_{2D}, and E_{3D}, with the 2-D model representing the data well. Similar agreement using E_{2D} has been found for PGSE experiments on water in bilayers of the polycrystalline smectic liquid crystal, sodium 4-(1'-heptylnonyl)benzenesulphonate [64].

Of course, the echo-attenuation expressions for self-diffusion in a randomly oriented array of dimensionally restricted pores contain an approximation, namely that displacements in the restricted dimensions are ignored. More exact expressions, in which these displacements are accounted for, have been derived by Mitra and Sen [65] using the appropriate eigenmode expansions for the solution to the diffusion equation for liquid molecules in pipes of radius a and between parallel sheets of separation a. Their echo-attenuation relationships are

$$E_{2D} = \exp(-q^2 D\Delta) \int_0^1 \exp\left[q^2 \left(D\Delta - \langle r_\perp(\Delta)^2\rangle/2\right) x^2\right] dx \tag{6.92}$$

with

$$\langle r_\perp(\Delta)^2\rangle/2 = \frac{a^2}{3}\left[1 - \exp(-3D\Delta/a^2)\right] \tag{6.93}$$

while for an array of randomly oriented pipes,

$$E_{1D} = \exp(-q^2 D\Delta) \int_0^1 \exp\left[q^2 \left(D\Delta - \langle r_\perp(\Delta)^2\rangle/4\right) (1 - x^2)\right] dx \tag{6.94}$$

with

$$\langle r_\perp(\Delta)^2\rangle/4 = \frac{a^2}{4}\left[1 - \exp(-4D\Delta/a^2)\right] \tag{6.95}$$

D being, in each case, the free molecular self-diffusion coefficient. Note that Δ_r is now replaced by Δ, since the narrow gradient pulse condition is required to derive these equations.

6.6.4 Curvilinear diffusion

Motion without branches

Figure 6.21 shows an echo-attenuation plot [63] for water protons in a sample of Aerosol OT/water, a lamellar phase lyotropic liquid crystal system with random domain orientation. The PGSE experiment reveals an interesting behaviour as D is increased. At short times the data exhibit a dependence on g and Δ, as given by the 2-D polydomain expression, E_{2D}, of eqn 6.90. At longer times the diffusion rate is apparently slower, and the curvature of $E(q)$ vs q^2 reduces, indicating that the diffusion behaviour is tending towards 3-D. For Δ sufficiently short that the water molecules reside in a single local domain with characteristic director orientation, the behaviour E_{2D} is expected. As Δ becomes sufficiently large for the molecules to move to new domains of differing orientation, their motion becomes more 3-D in character. The curious feature of this experiment is that the apparent diffusion coefficient reduces with time.

In the experiment described, we measure molecular displacements in the laboratory frame, but the diffusion, at a microscopic level, is occurring in a curvilinear coordinate system. A similar problem exists in considering the reptational diffusion of a polymer molecule in the curvilinear tube formed by impeding neighbours. It was shown by de Gennes [66] and Edwards [67] that such a motion leads to a dependence of laboratory-frame mean-square displacement on $t^{1/2}$ instead of the usual t-dependence of unrestricted diffusion. A detailed discussion of this problem is found elsewhere [68], but a simple picture can be gained as follows.

Consider molecular motion confined to one- or 2-D local elements. These elements have rms length λ, and are interconnected such that the diffusing particle migrates from one randomly oriented element to another, tracing out a random walk in the laboratory frame as illustrated in Fig. 6.22, with end-to-end distance R. A key factor in this motion is the lack of branch points and the consequent confinement of the particles to specific, albeit tortuous, paths. Suppose we define a total rms curvilinear

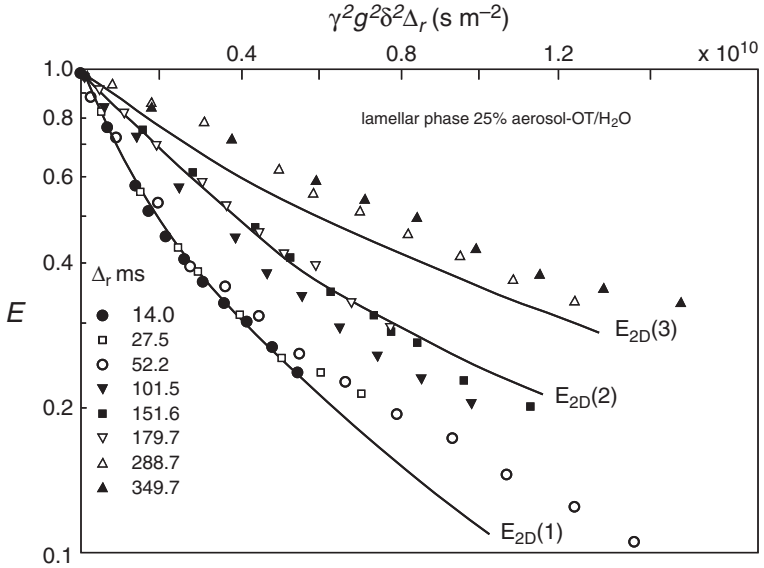

Fig. 6.21 Echo-attenuation plot for a 25% sample of Aerosol OT/water showing dependence of diffusive behaviour as Δ_r is varied over a wide range. For spins residing in one domain only, the data should be coincident. The theoretical curves, $E_{2D}(N)$ correspond to molecules diffusing successively in N domains. (Data taken from reference [63].)

path length Λ, comprising N elements with diffusion time t and local self-diffusion coefficient, D. For 1-D motion we have

$$\Lambda^2 = 2Dt = N^2\lambda^2 \tag{6.96}$$

In the laboratory frame

$$\overline{R^2} = N\lambda^2 = 2DN^{-1}t = \lambda(2Dt)^{1/2} \tag{6.97}$$

The case of two-dimension local diffusion is treated identically, but with a coefficient of 4 rather than 2 appearing in eqn 6.96. Given that we expect $\overline{R^2} = 6D_{\text{eff}}t$, we have for 1-D curvilinear diffusion

$$D_{\text{eff}} = \frac{1}{3}DN^{-1} \tag{6.98}$$

and for the 2-D case

$$D_{\text{eff}} = \frac{2}{3}DN^{-1} \tag{6.99}$$

The distribution of laboratory displacements in such curvilinear diffusion is Gaussian provided N is large, but the dependence of $\overline{R^2}$ as $t^{1/2}$ rather than t is distinctly non-Brownian. In the PGSE experiment the echo signal $E(q)$ will exhibit the usual Gaussian dependence on q but with an effective diffusion coefficient which decreases as $\Delta^{-1/2}$. The data shown in Fig. 6.21 correspond to an experiment in which N is small, so that the Gaussian behaviour is not reached as N increases. Expressions for

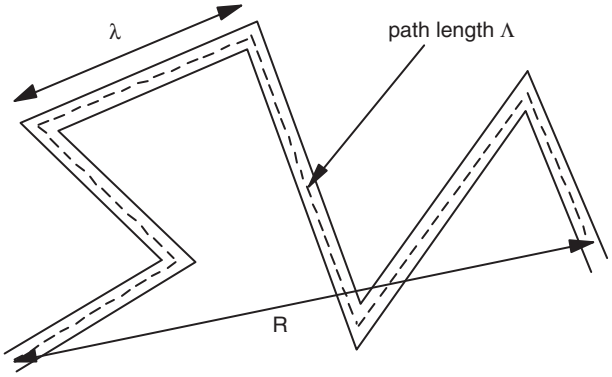

Fig. 6.22 One-dimensional curvilinear diffusion path without branching points, made up of local elements of rms length λ. The path length along the curvilinear path is Λ, while the direct end-to-end distance is R.

$E_{1D}(q)$ and $E_{2D}(q)$, appropriate where N is finite, are suggested in reference [63]. They consist of replacing D in both eqns 6.90 and 6.91 by DN^{-1}. In the limits $N = 1$ and $N \to \infty$, these equations reduce to the correct form. For finite N they do, in the relevant case of $E_{2D}(q)$, provide a good representation of the data shown in Fig. 6.21.

In the polymer problem, the curvilinear confinement exists only for the time, τ_d, taken for polymer to disengage from the tube [66, 68, 70, 71]. This means that the $\overline{R^2} \sim \Delta^{1/2}$ behaviour can only be observed if Δ is less than τ_d and where q is sufficiently large for the PGSE experiment to detect molecular displacements smaller than the rms dimensions of the polymer, the so-called semi-local motion. In principle this is just a matter of making g or δ large enough. Because of T_2 relaxation, the magnitude of δ is constrained. Given the largest available polymers, the measurement of semi-local motion requires gradient strengths in excess of $10\,\mathrm{Tm}^{-1}$. Figure 6.23 shows an example of mean-squared displacements measured for entangled high molecular weight polymers in semi-dilute solution, at times $t > \tau_d$, where $Z^2 \sim t$, and $t < \tau_d$, where $Z^2 \sim t^{1/2}$. At even shorter NMR observation times, $t = \Delta$, the Rouse time, is reached, where a transition to $Z^2 \sim t^{1/4}$ is observed. By selecting different molar masses, the Rouse and reptation times can be 'tuned' to bring the relevant dynamical regime into the PGSE NMR 'window'.

Motion with branches

Tube disengagement is an example of branching in the paths available for the molecule. Suppose that instead of confinement to a fixed curvilinear path, the diffusing molecule has a choice of paths after moving N_0 elements for a mean-square distance R_0^2 in the lab frame over a time τ. This yields a timescale-independent, laboratory-frame self-diffusion coefficient, D_{eff}, of $R_0^2/6\tau$. Equation 6.97 then yields a particularly simple result,

$$D_{\mathrm{eff}} = \begin{cases} \frac{D}{3N_0} & \text{for 1-D local motion,} \\ \\ \frac{2D}{3N_0} & \text{for 2-D local motion.} \end{cases} \tag{6.100}$$

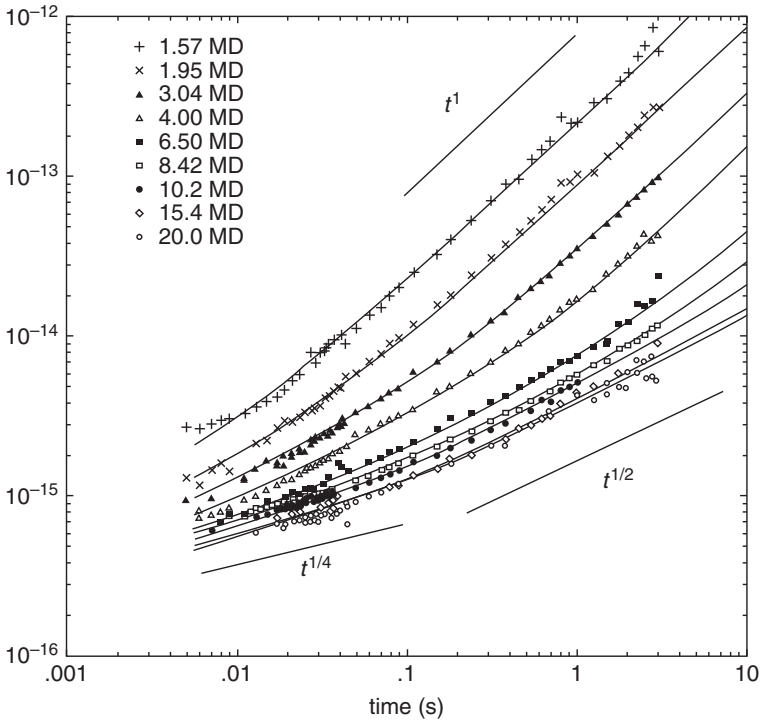

Fig. 6.23 $log(Z^2)$ vs $log(t)$, for nine different molar mass polystyrenes in semi-dilute solution. Asymptotic scaling exponents are shown in the straight-line tangents. Clear $t^{1/4}$ to $t^{1/2}$ and $t^{1/2}$ to t^1 transitions are apparent as the changing molar masses sweep the Rouse and tube disengagement times across the NMR window. From reference [69].

The 1-D expression leads to the well-known $D_{\text{eff}} \sim M^{-2}$ 'reptation law' for polymers, where M is the molar mass.[7] However eqn 6.100 is generally applicable to a wide class of problems, including the diffusion of small molecules in liquid crystals or emulsions. One specific limit of interest is the case $N = 1$, which corresponds to unidirectional motion between branch points. This is equivalent to the curvilinear diffusion problem, but where branching options exist on entering the next domain. Where the motion is locally 1-D or 2-D, D_{eff} is, respectively, $\frac{1}{3}D$ or $\frac{2}{3}D$. Examples of such behaviour have been found for diffusion in microemulsions [72].

6.6.5 Anisotropic diffusion in oriented liquid crystals

One of the problems associated with trying to measure anisotropic diffusion in liquid crystal environments concerns the effect of significant line-broadening caused by dipolar and quadrupolar interactions. When cubic symmetry is broken by the orientational order associated with a lyotropic or thermotropic liquid crystalline phase, these

[7] $M \sim N_0$. The 1-D diffusion coefficient D is inversely proportional to the total polymer friction along the curvilinear path, i.e. $D \sim N_0^{-1}$.

interactions are no longer averaged to zero, no matter how fast the probe molecule is diffusing in the mesophase environment. The problem is most severe in thermotropic liquid crystals where one wishes to measure the diffusion of the nematogen. However there does exist a solution, albeit one that requires great experimenter skill and care. What is required is to 'narrow the line' using multiple pulse RF methods, as outlined in Section 4.6.3. The art of the method is to find a way of inserting magnetic field gradient pulses into the mix, so as to produce the desired sensitivity to diffusion.

The first example of the application of PGSE methods to examine diffusion anisotropy in thermotropic liquid crystals was by the Ljubljana group of Blinc *et al.* [73, 74], who used multiple pulse line narrowing techniques to extend the transverse coherence of the liquid crystal spin magnetisation over a timescale sufficient to measure diffusion. These experiments required the gradient pulses to be only a few microseconds long and applied in specific 'windows' of the multiple pulse sequence [73, 75–77].

The 'Achilles heel' when measuring diffusion using multiple pulse line narrowing is this need to apply pulsed gradients in the narrow time windows (on the order of 10 microseconds) of the RF pulse sequence. In consequence, the available gradient strength is limited, and slow diffusion is difficult to access. One brute-force alternative is to use multiple-pulse decoupling in conjunction with a large, although static, magnetic field gradient, an approach used to measure slow diffusion in plastic crystals [78]. The presence of the gradient ensures that the RF pulses are slice-selective by default, a point discussed again in Section 12.2.6. However, there are deeper problems to be addressed when gradients are present during the RF pulse transmission. Clearly, different parts of the sample experience different magnetic field strengths, leading to a position-dependent resonance frequency offset across the sample space. This causes a corresponding variation of the decoupling efficiency, with resulting signal-to-noise ratio loss, and, in addition, the applied magnetic field gradient is scaled by the scaling factor of the decoupling sequence that reduces Zeeman spin operator terms such as chemical shift [79] (see Section 4.6.3). The latter effect means that the effective gradient experienced by spins becomes inhomogeneous across the sample, leading to an inhomogeneous attenuation of the signal by diffusion.

Dvinskikh and Furó [79, 80] have proposed an elegant means of reducing the influence of the variation of the decoupling effect by using a controlled slice selection, thus cancelling the signal from regions with large resonance offset so that the measurement is representative of that part of the sample where the Zeeman scaling factor is well defined. Their pulse sequence, based on MREV-8, is shown in Fig. 6.24(a). They choose to perform the slice selection before the PGSE sequence by applying a soft inversion pulse, this pulse being absent in every second scan so that when two subsequent FIDs are subtracted, signal from longitudinal magnetisation in the selected slice is summed, while that arising from outside the region is cancelled. By adjusting the width of the excited slice, they can control the Zeeman scaling factor to any required accuracy. Here the gradient amplitude and duration are kept constant, and the diffusion time Δ varied. Dvinskikh and Furó applied the method to ^{19}F spins in caesium perfluoroctanoate/D_2O (50 wt %), using the known chemical shifts of the ^{19}F spins to confirm that the Zeeman scaling factor agreed with the theoretical MREV-8 value of $\frac{\sqrt{2}}{3}$. Figure 6.24(b) shows the PGSE NMR echo attenuation (as a function of Δ)

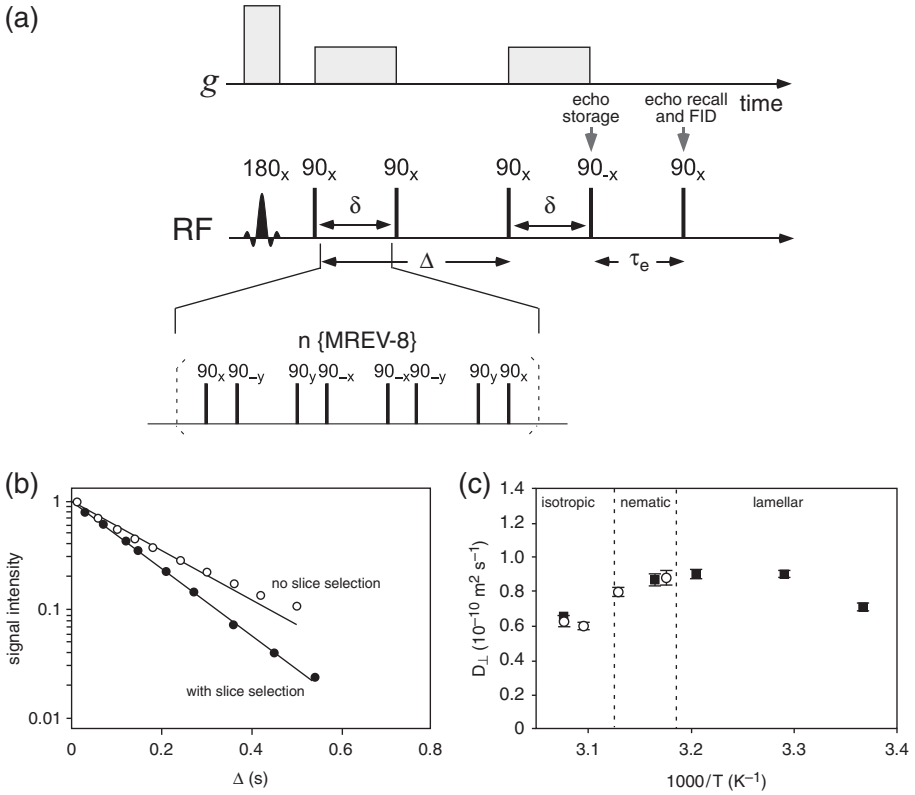

Fig. 6.24 (a) Pulse sequence for stimulated-echo PGSE NMR combined with MREV-8 in which a longitudinal eddy current delay (LED) period, τ_e is included. Slice selection is performed using a prior 180° inversion RF pulse, which is absent every second scan, so that subtraction of alternate signals leads to signal from the desired slice. (b) Application of the pulse sequence to ^{19}F spins in caesium perfluoroctanoate/D_2O, showing the echo attenuation with and without slice selection. (c) Measured $D_\perp$ for the perfluoroctanoate across the phase diagram. (Adapted from Dvinskikh and Furó [79].).

for measurements obtained without and with slice selection. In the latter case, a more uniform gradient results, consistent with the known Zeeman scaling factor.

6.6.6 Diffusion in fractal geometries

Natural structures often exhibit fractal character [81–85] in which self-similarity and non-integer dimensionality play a role. A nice example of fractal behaviour is found in the geography of coastlines [82]. The appearance of a coastline is similarly indented and tortuous, whether viewed from an orbiting satellite or from a distance of a few metres. This self-similarity (sometimes called dilation symmetry) is consistent with a shape that is scale independent. One of the consequences of this is that the total coastline length depends on the smallest step, ϵ, used in its measurement. If the total number of ϵ-intervals in the measurement is $N(\epsilon)$ and the total length is $L(\epsilon)$ then

$$N(\epsilon) \sim F\epsilon^{-d} \tag{6.101}$$

and

$$L(\epsilon) \sim F\epsilon^{1-d} \tag{6.102}$$

where d is called the similarity dimension. A non-fractal coastline would have $d = 1$, whereas fractal behaviour is exhibited when $d > 1$.

Porous materials exhibit analogous behaviour in the volume and surface organisation. Here d tells us the dependence of the 'measure' on the length dimension. In Euclidean behaviour we expect that the total pore volume within a radius R would vary as R^3. 'Volume fractal' behaviour is typified by $V \sim R^d$, where $1 \leq d \leq 3$. 'Surface fractal' behaviour is typified by $S \sim R^d$, where $1 \leq d \leq 2$.

The Brownian random walk provides a very good example of fractal behaviour, a wandering plane-filling 'coastline' in which $d = 2$. Consider a particular walk of end-to-end rms distance r. As ϵ decreases $N \sim F\epsilon^{-d}$. F can be determined as r^d from the result $N = 1$ when $\epsilon = r$. Thus $r \sim N^{1/d}$ and so yields the familiar random walk result, $r \sim N^{1/2}$, when $d = 2$. In fact this same dimensionality applied when the random walk is performed in 3-D space. Note that the fractal dimension associated with the random walk is different to that describing, for example, volume fractal behaviour, and is assigned the symbol d_w. An interesting example is the self-avoiding random 'walk' that defines the random coil polymer conformation in the solution phase [40], for which the chain end-to-end distance scales as $r \sim N^{3/5}$, giving $d = 5/3$.

Self-diffusion is very sensitive to the dimensional character of the path taken via the dependence of rms distance on time, this parameter being directly proportional to N. The fractal character may be defined by the relation [86–88]

$$\overline{r^2} = 6Dt^{2/(2+\theta)} \tag{6.103}$$

in which θ determines the effective dimensionality of the random walk, reducing to zero in the case of Brownian motion. A timescale-dependent self-diffusion experiment can be used to measure θ, and this quantity may be related to the volume fractal dimension [86–88], an effect that can be exploited in the PGSE experiment. From the relation $E = \exp(-\frac{1}{2}\gamma^2 g^2 \delta^2 \overline{Z^2})$, the fractal dimension enters [37, 89–91] through the term $\overline{Z^2}$ as $\Delta^{2/(2+\theta)}$, giving

$$E(q, \Delta) = \exp(-\gamma^2 g^2 \delta^2 D^{2/(2+\theta)}) \tag{6.104}$$

Note that the fractal dimension relates to the migration space of the spins. Where the material exhibits fractal surfaces but the molecules diffuse in a non-fractal (Euclidean) volume, the PGSE experiment exhibits the usual Brownian behaviour. In such an system the fractal behaviour is only apparent when the experimental parameter is surface-dependent, an example being the relaxation of spins due to the existence of surface magnetisation 'sinks' [92–94].

6.7 Frequency-domain measurements and restricted motion

In Chapter 5, the concept of frequency-domain modulated gradient NMR measurement of translational motion was introduced. Using a periodic effective gradient waveform,

the induced time-dependent signal attenuation, $\exp(-\beta(t))$, can be related to the spectrum, $\underline{\underline{D}}(\omega)$, of the velocity autocorrelation function, $\langle \mathbf{u}(\tau)\mathbf{u}(0)\rangle$, where $\mathbf{u}$ has zero time average, such that the total velocity is $\mathbf{v} = \mathbf{u} + \langle \mathbf{v}\rangle$. The mean flow, $\langle \mathbf{v}\rangle$, introduces a time-dependent phase shift, $\exp(-i\alpha(t))$. These relationships are outlined in detail in section 5.7.2.

The question of interest in the present context is how the effect of restricted diffusion imprints the velocity autocorrelation spectrum and may be thereby observed in the echo attenuation. The particular details of the gradient pulse train used need not concern us here, although the use of a CPMG train under steady or pulsed gradient conditions is the most convenient to use, leading to the simple result $\beta(t) = \frac{1}{2}NT\gamma^2 g^2 T^2 D_{zz}(2\pi/T)$, where $t = NT$ and z is the gradient axis. The challenge is therefore to find the appropriate velocity autocorrelation spectrum, $D_{zz}(\omega)$.

In seeking $D_{zz}(\omega)$, it is helpful to note two important relations that follow from eqn 1.58. First

$$D_{zz}(\omega = 0) = \lim_{t\to\infty} \int_0^t < u_z(\tau)u_z(0) > d\tau. \tag{6.105}$$

and

$$\langle u_z(t)u_z(0)\rangle = \frac{1}{2}\frac{\partial^2\langle Z_u(t)^2\rangle}{\partial t^2} \tag{6.106}$$

the total displacement, $Z(t)$, being composed of $Z_u(t) + \langle v_z\rangle t$. Where $Z_u(t)$ has zero time average and zero ensemble average, it is follows that[8]

$$\begin{aligned}\langle v_z(t)v_z(0)\rangle &= \frac{1}{2}\frac{\partial^2\langle Z(t)^2\rangle}{\partial t^2} \\ &= \frac{1}{2}\frac{\partial^2\langle Z_u(t)^2\rangle}{\partial t^2} + \langle v_z\rangle^2 \\ &= \langle u_z(t)u_z(0)\rangle + \langle v_z\rangle^2\end{aligned} \tag{6.107}$$

It is clear from eqn 6.107 that any estimation of the autocorrelation function of the mean-zero part of the velocity from the total time-dependent displacement, $Z(t)$, can be easily made by subtracting the flow contribution, as implied by the definition of $\beta(t)$ in eqn 5.128. In handling restricted diffusion, however, we only need focus on the stochastic contribution to displacement, $Z_u(t)$.

A knowledge of $\langle Z_u(t)^2\rangle$ therefore provides a starting point for calculating $\langle u_z(t)u_z(0)\rangle$, and hence its Fourier spectrum $D(\omega)$. Another route to $D(\omega)$ is from the initial standpoint of the time-dependent dispersion or diffusion coefficient $D(t)$ as defined by eqn 2.56, since

$$\langle u_z(t)u_z(0)\rangle = \frac{\partial}{\partial t}D(t) \tag{6.108}$$

This particular route turns out to be very convenient from a phenomenological standpoint, since one may often have a priori knowledge of long- or short-time limiting values of $D(t)$, as well as a knowledge of the characteristic times at which crossovers in diffusive behaviour occur, for example those times sufficient for molecules to diffuse known length scales.

[8]For the stationary ensemble $\langle Z(t)^2\rangle = \langle Z_u(t)^2\rangle + \langle v_z\rangle^2 t^2$

6.7.1 Spectral densities for free and restricted diffusion

Before considering restricted diffusion, it is helpful to examine the consequences of eqns 6.105 and 6.106 for free diffusion. The integration of eqn 6.105 requires a description of the mean-squared displacement at all times, including the ballistic regime of molecular collisions. From eqn 1.73, and denoting $t_\zeta = \gamma$, we may write

$$\begin{aligned} < u_z(t)u_z(0) > &= \frac{1}{2}\frac{\partial^2 \langle Z_u(t)^2 \rangle}{\partial t^2} \\ &= \frac{k_B T}{m}\exp(-\gamma t) \\ &= D_0 \gamma \exp(-\gamma t) \end{aligned} \tag{6.109}$$

The diffusion spectrum is the Lorentzian

$$D_{zz}(\omega) = D_0 \frac{1}{1+\omega^2/\gamma^2} \tag{6.110}$$

For free diffusion, the diffusion coefficient is a constant at all times in excess of γ^{-1}, and hence at all frequencies much lower than γ. The required result $D_{zz}(0) = D_0$ follows directly from eqns 6.105 and 6.110.

Phenomenological model for restricted diffusion

Restriction to diffusion leads to a reduction in the zero-frequency part of the $D_{zz}(\omega)$ spectrum. Given that the ballistic contribution to $< u_z(t)u_z(0) >$ is always present on the timescale of molecular collisions, the effect of boundary restrictions is to introduce velocity anti-correlation, a negative contribution to $< u_z(t)u_z(0) >$. The physical reason for anti-correlation is obvious. Collisions introduce velocity reversals. In consequence, the schematic form of the VACF where molecules are confined in a pore of size a will be via introduction of an additional negative term, such that

$$\langle u_z(t)u_z(0)\rangle = D_0\gamma\exp(-\gamma t) - D_0\tau_c^{-1}\exp(-t/\tau_c) \tag{6.111}$$

where τ_c is a time comparable with that required to traverse the pore, namely $\tau_c \sim a^2/D_0$. The corresponding spectrum is

$$D_{zz}(\omega) = D_0\frac{1}{1+\omega^2/\gamma^2} - D_0\frac{1}{1+\omega^2\tau_c^2} \tag{6.112}$$

For an interconnected porous medium where molecules experience wall collisions within pores, but on a longer timescale, experience an effective tortuosity-reduced diffusion coefficient $D_{\text{eff}}(\infty)$, we may write

$$\langle u_z(t)u_z(0)\rangle = D_0\gamma\exp(-\gamma t) - (D_0 - D_{\text{eff}}(\infty))\tau_c^{-1}\exp(-t/\tau_c) \tag{6.113}$$

and in consequence

$$D_{zz}(\omega) = D_0\frac{1}{1+\omega^2/\gamma^2} - (D_0 - D_{\text{eff}}(\infty))\frac{1}{1+\omega^2\tau_c^2} \tag{6.114}$$

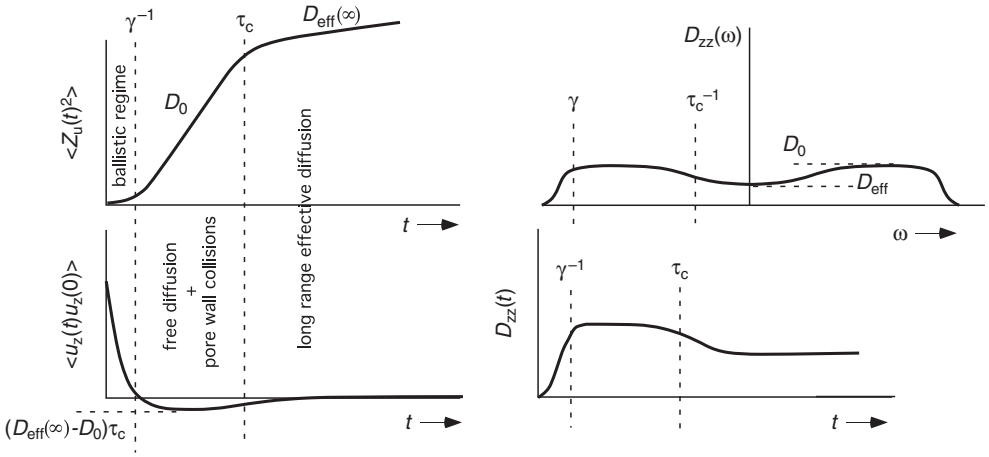

Fig. 6.25 Schematic of Z_u^2 and $\langle u_z(t)u_z(0)\rangle$ vs t, along with the associated diffusion spectrum $D_{zz}(\omega)$ and time-dependent diffusion coefficient $D_{zz}(t)$, in the case of an interconnected porous medium. For an enclosing pore, $D_{\text{eff}}(\infty) = 0$. Note that this simple picture applies only when $\tau_c \gg \gamma^{-1}$.

and, by eqn 2.56,

$$D_{zz}(t) = D_0\,(1 - \exp(-\gamma t)) - (D_0 - D_{\text{eff}}(\infty))\,(1 - \exp(-t/\tau_c)) \tag{6.115}$$

This picture is illustrated schematically in Fig. 6.25. Note that the size of the negative term in the velocity autocorrelation function is much smaller than that associated with ballistic collisions, by the ratio γ^{-1}/τ_c. However, because of the integration to obtain $D_{zz}(0)$ over the correlation time associated with wall collision effects, its effect is significant.

Plane parallel boundaries

In the case of plane parallel boundaries separated by a, where diffusion is measured normal to the walls, there exists an exact expression [95] for the velocity autocorrelation function. In the limit $\tau_c \gg \gamma^{-1}$,

$$\langle u_z(t)u_z(0)\rangle = D_0\gamma\exp(-\gamma t) - \frac{4D_0^2}{a^2}\sum_{k=-\infty}^{\infty}\exp(-(2k+1)^2\pi^2 D_0 t/a^2) \tag{6.116}$$

The zero-frequency (long-time) diffusion coefficient is indeed zero because of the identity $\sum_{k=-\infty}^{\infty}\pi^{-2}(2k+1)^{-2} = \pi^2/4$.

Undulating lamellae

Diffusion normal to plane parallel boundaries has been studied using FDMG NMR [96] in the case of a lamellar phase lyotropic liquid crystal, in the limit $t \gg \tau_c = d^2/2D_0$ where d is the spacing between the layers. Water molecules diffusing in the interlamellar layer will, for times in excess of τ_c, be confined to 2-D diffusion, $D_\perp$. However

where undulations in the lamellae are present, such transverse diffusion converts $\perp$ displacements into displacements normal to the bilayer. Furthermore, undulation fluctuations will carry water molecules, providing an additional mechanism for movement in the direction of the layer normal. In this study, the diffusion spectrum measured in this normal direction gave access to the characteristic bilayer undulation rates and amplitudes.

Multilamellar vesicles

One of the particular advantages of the FDMG NMR method, especially using the Carr–Purcell train variant, is the opportunity to refocus all coherent phase shifts due to flow. This has particular application in the case of rheo-NMR, where a non-uniform flow field has the effect of introducing phase-spreading and echo train attenuation. Hence the FDMG NMR method has the potential to remove these velocity shear effects, revealing decay due to diffusion alone. One example of the application of this approach is in the measurement of the size of multi-lamellar onion vesicles (MLVs) under shear.

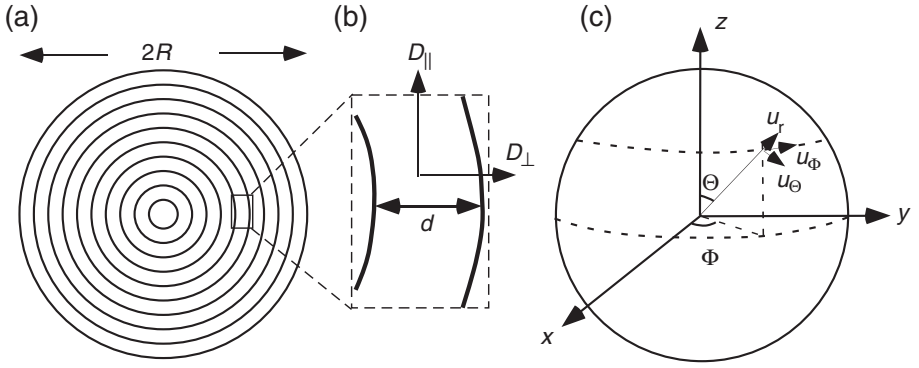

Fig. 6.26 A multilamellar vesicle. (a) The interlayer spacing value $d \sim 10^{-8}$m leads to a time, τ_c, for diffusion perpendicular to the membranes, $\sim 10^{-8}$ s, which is unobservable by FDMG NMR. (b) The much larger onion size $R \sim 10^{-6}$ m leads diffusion parallel to the membranes with decay time, $\tau_d \sim 10^{-3}$ s. The gradient is assumed to be applied along the z-direction, as in (c).

MLVs are formed from certain lyotropic lamellar phases under shear. Providing the shear rate is sufficiently high, spherical vesicles may be formed by shear-induced buckling of the membranes [97] and onion formation has been confirmed experimentally using various techniques and chemical systems [97–99]. Onion size estimation is based on measuring the restricted diffusion of inter-lamellar water molecules using the FDMG NMR sequence [100]. Figure 6.26 shows the coordinate system for the MLV onion, with the multi-bilayer structure, a chosen shell of radius r in which a local section of water layer is shown. Diffusion may be described respectively perpendicular and parallel to the bilayer normals as $D_\perp(t)$ and $D_\parallel(t)$. In the NMR experiment the magnetic field gradient used to encode for motion is applied along some pre-determined z-axis. For diffusion along z, the displacements are azimuth-independent and given by

$$D_{zz}(t,\Theta) = D_{\perp}(t)\cos^2\Theta(t) + D_{\parallel}(t)\sin^2\Theta(t) \tag{6.117}$$

The velocity autocorrelation function follows from proposing a time-dependent diffusion coefficient in accordance with eqn 2.56. At the shortest time ($t \ll \tau_c = d^2/2D_0$), few water molecules will have a chance to collide with the bilayer, and so $D_{\parallel}(t)$ and $D_{\perp}(t)$ reduce to the free diffusion coefficient D_0 of the solvent. At longer times, molecules encounter the bilayers in their displacements perpendicular to the membranes and to encompass this phenomenologically, we may write

$$D_{\perp}(t,\Theta) = D_{perm} + (D_0 - D_{perm})\exp(-t/\tau_c) \tag{6.118}$$

where D_{perm} is the diffusion coefficient corresponding to permeation of the water molecules through the various defects present on the membranes. While the limits of eqn 6.118 are correct, details of the crossover are approximate. Nonetheless the essential physics is represented in terms of a mathematical function that is easily handled in subsequent analytic manipulations. This simple device applies in the higher timescale hierarchies as well.

Of course, one needs to sum contributions from all (Θ, Φ) segments in each of the shells of radius r. Provided that diffusion distances are sufficiently short that a unique angle Θ can be ascribed to each water molecule, we may write:

$$\begin{aligned}
\langle D_{zz}(t)\rangle &= \frac{\int_0^{\pi} D_{zz}(t,\Theta)P(\Theta)d\Theta}{\int_0^{\pi} P(\Theta)d\Theta} \\
&= \frac{\int_0^{\pi} \left(D_{\perp}(t)cos^2\Theta(t) + D_{\parallel}(t)sin^2\Theta(t)\right) sin\Theta d\Theta}{\int_0^{\pi} sin\Theta d\Theta} \\
&= \frac{1}{3}\left[D_{perm} + (D_0 - D_{perm})\exp(-t/\tau_c) + 2D_0\right]
\end{aligned} \tag{6.119}$$

where $P(\Theta)$ is the polar angle distribution.

Allowing for longer times in which water molecules explore differing Θ coordinates, the expression becomes more complex. However, a simpler approach is possible [100], again using limiting-case expressions. For $t \gg \tau_d(r) = r^2/2D_0$, $D_{zz}(t)$ must reach the limit D_{perm}, since only permeation through the bilayers can permit diffusion on a greater distance than r. Using the same phenomenological approach

$$\langle D_{zz}(t)\rangle = D_{perm} + \frac{1}{3}(D_0 - D_{perm)})(\exp(-t/\tau_c) + 2\exp(-t/\tau_d(r)) \tag{6.120}$$

Finally, the integration over shell size $0 < r < R$ must be performed where R is the onion size. This demands some allowance for permeation effects between layers. An analysis of the relative timescales for permeation and diffusion around the entire spherical shell suggests that it is reasonable to assume a single correlation time, $\tau_d(r)$, for each shell over the time to diffuse the dimensions of the onion. Hence one may average NMR signals acquired from layers with different r values rather than average $\tau_d(r)$ itself across the distribution of layers. Based on a calculation of the diffusion spectrum for a single shell and making radial averaging the final step, a closed-form expression results [100].

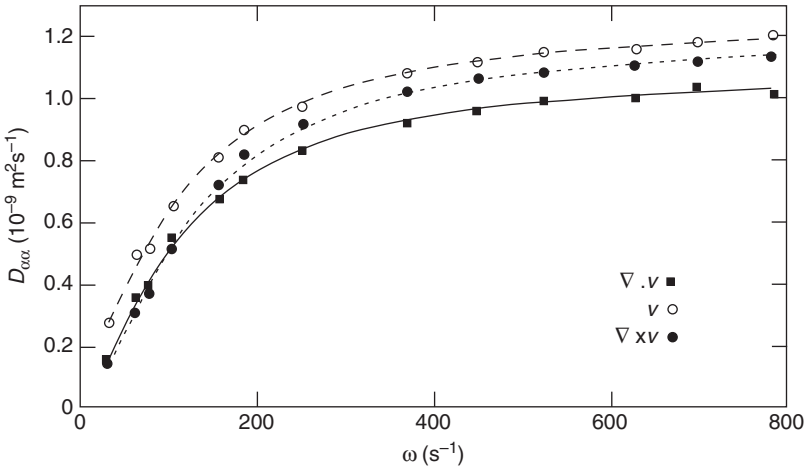

Fig. 6.27 Diffusion spectrum of an onion phase: diffusion is measured along the flow-gradient ($\nabla\mathbf{v}$), flow ($\mathbf{v}$), and vorticity ($\nabla \times \mathbf{v}$) directions. The solid lines are fits to the analytic $D(\omega)$, and give independent D_{perm} ($\sim 10^{-10}m^2s^{-1}$) and onion radius values ($\sim 7\mu m$) for each direction. (Adapted from reference [100].)

6.7.2 Spectral analysis of flow

Frequency-domain modulated gradient NMR methods based on CPMG echo trains are well suited to the study of the dispersion spectrum for complex flow. In particular, for Péclet numbers in excess of unity, the displacements are generally larger that experienced in purely diffusive motion, and this proves particularly useful given the tendency of the CPMG sequence to reduce sensitivity to diffusive effects. Furthermore, the frequencies that can be accessed by FDMG NMR (from hertz to kilohertz) may be well tailored to characteristic flow times. One example of the application of these methods has been in the study of transverse 'meandering' motion for flow through a beadpack [101]. Figure 6.28 shows a schematic representation of the phenomenon.

Applying the magnetic field gradients in the direction transverse to the mean flow, for water flowing in a monodisperse latex bead pack (diameter 50 microns) and at Péclet numbers ranging from 10 to 5000, these authors observe spectral peaks at a frequency corresponding to the inverse time for flow around a bead, an effect they attribute to coherent meandering flow around the bead. These spectra agree very well with those calculated from lattice Boltzmann simulations [102] in which negative velocity autocorrelation function transients are seen. Similar agreement was found using a range of bead packs comprising different bead diameters, lending credence to the interpretation.

Representing the transverse component of meandering flow by a simple oscillatory motion with frequency $2/\tau_v$, where the characteristic flow time $\tau_v = d/v$, d being the bead diameter and v the local fluid velocity of mean $\langle v \rangle$, a simple velocity autocorrelation function was derived in which both meandering flow and dispersion were accommodated,

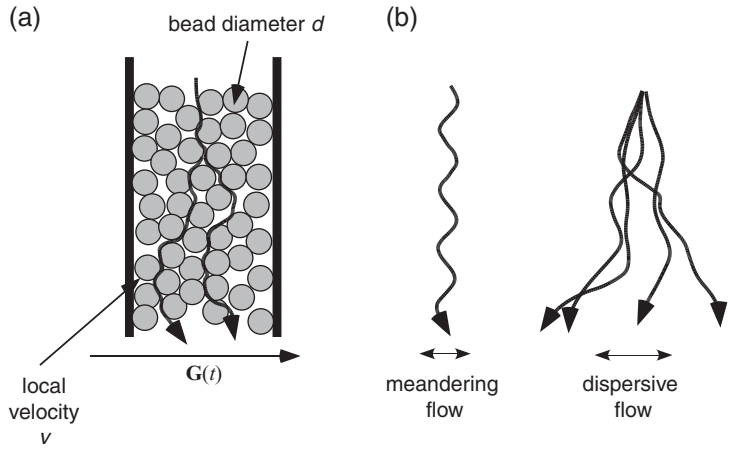

Fig. 6.28 Meandering flow superposed on dispersion for water flowing through a bead pack. The time-dependent gradient is applied transverse to the mean flow direction. (Adapted from reference [101].)

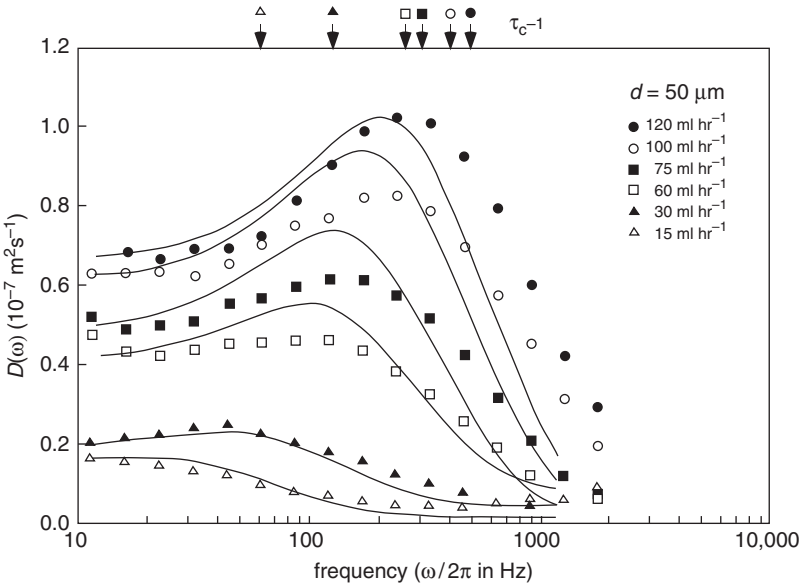

Fig. 6.29 The effective transverse dispersion coefficients, $D(\omega)$, measured at each frequency $f = 1/T$ for the FDMG NMR sequence of Fig. 5.32(b), over the range of flow rates as shown, for a 50-micron bead pack. The theoretical fits are obtained using the velocity autocorrelation functions of Maier *et al.* [102]. (Adapted from reference [101].)

$$\langle u(t)u(0)\rangle = D_0\gamma\exp(-t\gamma) + \int_0^\infty (bv^2)P(v)\exp(-t/\tau_v)dv$$
$$+\frac{1}{2}\int_0^\infty a^2v^2P(v)cos(2t/\tau_v)dv \qquad (6.121)$$

a and b being coefficients of order unity, and $P(v)$ the local velocity distribution, taken to be Gaussian with standard deviation σ. This leads to a diffusion spectrum

$$D(\omega) = D_0 + b\int_0^\infty P(v)\frac{dv}{1+\omega^2\tau_v^2}dv + \\ +\frac{1}{4}a^2(2\pi\sigma^2)^{-1/2}(d/2)^3\exp(-(\omega d/2 - \langle v\rangle)^2/2\sigma^2) \qquad (6.122)$$

This simple model provides a good representation of the essential features of Fig. 6.29 and, in particular, the presence of a peak at a frequency corresponding to the inverse time for flow around a bead. The use of such frequency-domain methods for the analysis of translational motion clearly has considerable potential for identifying coherent flow phenomena in otherwise complex, semi-random flow structures.

References

[1] D. E. Woessner. NMR spin-echo self-diffusion measurements on fluids undergoing restricted diffusion. *J. Phys. Chem.*, 67:1365, 1963.

[2] D. S. Grebenkov. Use, misuse, and abuse of apparent diffusion coefficients. *Concepts in Magnetic Resonance*, 36A:24, 2010.

[3] J. Bear. *Dynamic of Fluids in Porous Media*. Elsevier, New York, 1972.

[4] P. N. Sen, L. M. Schwartz, P. P. Mitra, and B. I. Halperin. Surface relaxation and the long time diffusion coefficient in porous media: periodic geometries. *Phys. Rev. B*, 49:215, 1994.

[5] P-Z. Wong. *AIP conference proceedings 154*, chapter Physics and Chemistry of Porous Media II. AIP, New York, 1990.

[6] J. W. Haus and K. W. Kehr. Diffusion in regular and disordered lattices. *Phys. Rep.*, 150:263, 1987.

[7] T. de Swiet and P. N. Sen. Time dependent diffusion coefficient in a disorded medium. *J. Chem. Phys.*, 104:206, 1996.

[8] R. W. Mair, P. N. Sen, M. D. Hürlimann, S. Patz, D. G. Cory, and R. L. Walsworth. The narrow pulse approximation and long length scale determination in xenon gas diffusion NMR studies of model porous media. *J. Magn. Reson.*, 156:202, 2002.

[9] P.T. Callaghan, A. Coy, L. C. Forde, and C. J. Rofe. Diffusive relaxation and edge enhancement in NMR microscopy. *J. Magn. Reson. A*, 101:347, 1993.

[10] P.P Mitra, P.N. Sen, L.M. Schwartz, and P. Le Doussal. Diffusion propagator as a probe of the structure of porous media. *Phys. Rev. Lett.*, 68:3555, 1992.

[11] P. P. Mitra, P. N. Sen, and L. M. Schwartz. Short time behaviour of the diffusion coefficient as a geometrical probe of porous media. *Phys. Rev. B*, 47:8565, 1993.

[12] George A. Baker Jr and Peter Graves-Morris. *Pade Approximants*. Cambridge University Press, New York, 1996.

[13] L. L. Latour, P. P. Mitra, R. L. Kleinberg, and C. H. Sotak. Time-dependent diffusion coefficient of fluids in porous media as a probe of surface-to-volume ratio. *J. Magn. Reson. A*, 101:342, 1993.

[14] L.J. Zielinski and P. N. Sen. Effects of finite-width pulses in the pulsed-field gradient measurement of the diffusion coefficient in connected porous media. *J. Magn. Reson.*, 165:153, 2003.
[15] J. R. Zimmerman and W. E. Brittin. Nuclear magnetic resonance studies in multiple phase systems: Lifetime of a water molecule in an adsorbing phase on silica gel. *J. Phys. Chem.*, 61:1328, 1957.
[16] W. Feller. *Probability Theory and Its Application*. Wiley, New York, 1950.
[17] H. Wennerstrom. Nuclear magnetic relaxation induced by chemical exchange. *Mol. Phys.*, 24:69, 1972.
[18] Paul A. Bottomley, Thomas H. Foster, Raymond E. Argersinger, and Leah M. Pfeifer. A review of normal tissue hydrogen NMR relaxation times and relaxation mechanisms from 1–100 MHz: Dependence on tissue type, NMR frequency, temperature, species, excision, and age. *Med. Phys.*, 11:425, 1984.
[19] E. E. Burnell, M. E. Clark, J. A. M. Hinke, and N. R. Chapman. Water in barnacle muscle. III. NMR studies of fresh fibers and membrane-damaged fibers equilibrated with selected solutes. *Biophys. J.*, 33:1, 1981.
[20] P. S. Belton, R. R. Jackson, and K. J. Packer. Pulsed NMR studies of water in striated muscle: I. Transverse nuclear spin relaxation times and freezing effects. *Biochim. Biophys. Acta.*, 286:16, 1972.
[21] B. M. Fung and T. W. McGaughy. The state of water in muscle as studied by pulsed NMR. *Biochim. Biophys. Acta.*, 343:663, 1974.
[22] S. N. Rustgi, H. Peemoeller, R. T. Thompson, D. W. Kydon, and M. M. Pintar. A study of molecular dynamics and freezing phase transition in tissues by proton spin relaxation. *Biophys. J.*, 22:439, 1978.
[23] G. B. Kolata. Water structure and ion binding: A role in cell physiology? *Science*, 192:1220, 1976.
[24] F. Franks. *Water: a Comprehensive Treatise, Vols 1–4*. Plenum, New York, 1972.
[25] W. Derbyshire. Heterogeneous systems. *Chem. Soc., Spec. Period. Rep. Nuclear Magnetic Resonance*, 5:264, 1978.
[26] W. Derbyshire. Heterogeneous systems. *Chem. Soc., Spec. Period. Rep. Nuclear Magnetic Resonance*, 7:193, 1978.
[27] K. J. Packer, D. A. T. Dick, and D. R. Wilke. The dynamics of water in heterogeneous systems. *Phil. Trans. R. Soc. London Ser. B*, 278:59, 1977.
[28] R. R. Knipsel, R. T. Thomson, and M. M. Pintar. Dispersion of proton spin-lattice relaxation in tissues. *J. Magn. Reson.*, 14:44, 1974.
[29] Seymour H. Koenig and Walter E. Schillinger. Nuclear magnetic relaxation dispersion in protein solutions: I. Apotransferrin. *J. Biol. Chem.*, 244:3283, 1969.
[30] O. K. Daszkiewicz, J. W. Hennel, B. Lubas, and T. W. Szczepkowski. Proton magnetic relaxation and protein hydration. *Nature*, 200:1006, 1963.
[31] P. J. Lillford, A. M. Clark, and D. V. Jones. Water in polymers. In *ACS Symposium Series*, volume 127, page 177, 1980.
[32] G. Held, F. Noack, V. Pollack, and B. Melton. Proton spin relaxation and mobility of water in muscle tissue. *Z. Naturforsch.*, 28c:59, 1973.
[33] J. M. Escayne, D. Canet, and J. Robert. Frequency dependence of water proton longitudinal nuclear magnetic relaxation times in mouse tissue at 20 C. *Biochim. Biophys. Acta.*, 721:305, 1982.

[34] S. H. Koenig, R. D. Brown, D. Adams, D. Emerson, and C. G. Harrison. Magnetic field dependence of 1/T1 of protons in tissue. *Invest. Radiol.*, 19:76, 1984.
[35] K. R. Brownstein and C. E. Tarr. Importance of classical diffusion in NMR studies of water in biological cells. *Phys. Rev. A*, 19:2446, 1979.
[36] Y-Q Song, L. Zielinski, and S. Ryu. Two-dimensional NMR of diffusion systems. *Phys. Rev. Lett.*, 100:248002, 2008.
[37] J. R. Banavar and L. M. Schwartz. *Molecular Dynamics in Restricted Geometries*, chapter Probing porous media with nuclear magnetic resonance, page 273. Wiley, New York, 1989.
[38] K.P. Whittall and A.L. Mackay. Quantitative interpretation of NMR relaxation data. *J. Magn. Reson.*, 84:134, 1989.
[39] M. Lipsicas, J.R. Banavar, and J. Willemsen. Surface relaxation and pore sizes in rocks—a nuclear magnetic resonance analysis. *Appl. Phys. Lett.*, 48:1544, 1986.
[40] P. G. de Gennes. Transfert d'excitation dans un milieu aléatoire. *C. R. Acad. Sci.*, 295:1061, 1982.
[41] L. M. Burcaw, M. W. Hunter, and P. T. Callaghan. Propagator-resolved 2D exchange in porous media in the inhomogeneous magnetic field. *J. Magn. Reson.*, 205:209, 2010.
[42] A. Abragam. *Principles of Nuclear Magnetism*. Clarendon Press, Oxford, 1961.
[43] K. J. Packer. The effects of diffusion through locally inhomogeneous magnetic fields on transverse nuclear spin relaxation in heterogeneous systems. proton transverse relaxation in striated muscle tissue. *J. Magn. Reson.*, 9:438, 1973.
[44] C. F. Hazelwood, D. C. Chang, B. L. Nichols, and D. E. Woessner. Propagator-resolved 2D exchange in porous media in the inhomogeneous magnetic field. *Biophys. J.*, 14:583, 1974.
[45] G. R. Coates, L. Xiao, and M. G. Prammer. *NMR Logging. Principles and Applications*. Halliburton Energy Services, Houston, 1999.
[46] Y-Q Song, S. Ryo, and P.N. Sen. Determining multiple length scales in rocks. *Nature*, 406:178, 2000.
[47] H. Cho and Y-Q Song. NMR measurement of the magnetic field correlation function in porous media. *Phys. Rev. Lett.*, 100:025501, 2008.
[48] B. Robertson. Spin-echo decay of spins diffusing in a bounded region. *Phys. Rev.*, 151:273, 1966.
[49] C. H. Neuman. Spin-echo of spins diffusing in a bounded medium. *J. Chem. Phys.*, 60:4508, 1974.
[50] T. M. de Swiet and P. N. Sen. Decay of nuclear magnetization by bounded diffusion in a constant gradient. *J. Chem. Phys.*, 100:3597, 1994.
[51] M. D. Hürlimann, K. G. Helmer, T. M. de Swiet, and P. N. Sen. Spin echoes in a constant gradient in the presence of simple restriction. *J. Magn. Reson. A*, 113:260, 1995.
[52] S. D. Stoller, W. Happer, and F. J. Dyson. Transverse spin relqaxation in inhomogeneous magnetic fields. *Phys. Rev. A*, 44:7459, 1991.
[53] D. S. Grebenkov. NMR survey of restricted Brownian motion. *Rev. Mod. Phys.*, 79:1077, 2007.
[54] E. O. Stejskal. Use of spin echoes in a pulsed magnetic field gradient to study anisotropic, restricted diffusion and flow. *J. Chem. Phys.*, 43:3597, 1965.

[55] P. T. Callaghan and D. N. Pinder. Dynamics of entangled polystyrene solutions studied by pulsed field gradient nuclear magnetic resonance. *Macromolecules*, 13:1085, 1980.
[56] P. G. de Gennes. Dynamics of entangled polymer solutions I. Inclusion of hydrodynamic interactions, II. the Rouse model. *Macromolecules*, 9:587, 1976.
[57] J. Kärger, M. Kočiřik, and A. Zikánová. Molecular transport through assemblages of microporous particles. *J. Colloid and Interface Sci.*, 84:240, 1981.
[58] J. Kärger, H. Pfeifer, and W. Heink. Principles and applications of self-diffusion measurement by nuclear magnetic resonance. In *Advances in Magnetic Resonance, Vol. 12*. Academic Press, 1988.
[59] J. Kärger. Diffusionsuntersuchung von Wasser an 13X- sowie an 4A- und 5A-zeoliten mit hilfe der Methode der gepulsten Feldgradienten. *Z. Phys. Chem. (Leipzig)*, 248:27, 1971.
[60] H. Lechert. NMR investigations on the structure and sorption problems of Faujasite-type Zeolites. *Catal. Rev.*, 14:1, 1976.
[61] R. M. Barrer. *Zeolites and Clay Minerals as Sorbents and Molecular Sieves*. Academic Press, London, 1978.
[62] P. T. Callaghan, K. W. Jolley, and J. Lelievre. Diffusion of water in the endosperm tissue of wheat grains as studied by pulsed field gradient nuclear magnetic resonance. *Biophys. J.*, 28:133, 1979.
[63] P. T. Callaghan and O. Söderman. Examination of the lamellar phase of aerosol OT/water using pulsed field gradient nuclear magnetic resonance. *J. Phys. Chem.*, 87:1737, 1983.
[64] F. D. Blum, A. S. Padmanabhan, and R. Mohebbi. Self-diffusion of water in polycrystalline smectic liquid crystals. *Langmuir*, 1:127, 1985.
[65] P. P. Mitra and P. N. Sen. Effects of microgeometry and surface relaxation on NMR pulsed-field-gradient experiments: simple pore geometries. *Phys. Rev. B*, 45:143, 1992.
[66] P.G. de Gennes. Reptation of a polymer chain in the presence of fixed obstacles. *J. Chem. Phys.*, 55:572, 1971.
[67] M. Doi and S. F. Edwards. Dynamics of concentrated polymer systems. Part 1.—Brownian motion in the equilibrium state. *J. Chem. Soc., Faraday Trans. 2*, 74:1789, 1978.
[68] M. Doi and S. F. Edwards. *The Theory of Polymer Dynamics*. Oxford University Press, Oxford and New York, 1987.
[69] M. E. Komlosh and P. T. Callaghan. Segmental motion of entangled random coil polymers studied by pulsed gradient spin echo nuclear magnetic resonance. *J. Chem. Phys.*, 109:10053, 1998.
[70] P. G. de Gennes. *Scaling Concepts in Polymer Physics*. Cornell University Press, Ithaca and London, 1979.
[71] W. W. Graessley. Entangled linear, branched and network polymer systems—molecular theories. *Adv. Polymer Sci.*, 47:67, 1982.
[72] M. Clarkson, D. Beaglehole, and P. T. Callaghan. Molecular diffusion in a microemulsion. *Phys. Rev. Lett.*, 54:1722, 1985.
[73] R. Blinc, J. Pirs, and I. Zupancic. Measurement of self-diffusion in liquid crystals by a multiple-pulse NMR method. *Phys. Rev. Lett.*, 30:546, 1973.

[74] R. Blinc, M. Burgar, M. Luzar, J. Pirs, I. Zupancic, and S. Zumer. Anisotropy of self-diffusion in smectic-A and smectic-C phases. *Phys. Rev. Lett.*, 33:1192, 1974.

[75] L. Miljkovic, L. Thompson, M. M. Pintar, R. Blinc, and I. Zupancic. Self-diffusion in isotropic phase of para-alkoxybenzoic acid homologous series. *Chem. Phys. Lett.*, 38:15, 1976.

[76] M. Silva Crawford, B. C. Gerstein, A. L. Kuo, and C. G. Wade. Diffusion in rigid bilayer membranes. Use of combined multiple pulse and multiple pulse gradient techniques in nuclear magnetic resonance. *J. Am. Chem. Soc.*, 102:3728, 1980.

[77] M. I. Hrovat and C. G. Wade. NMR pulsed gradient diffusion measurements. 2. Residual gradients and lineshape distortions. *J. Magn. Reson.*, 45:67, 1981.

[78] I. Chang, G. Hinze, G. Diezemann, F. Fujara, and H. Sillescu. Self-diffusion coefcient in plastic crystals by multiple-pulse NMR in large static field gradients. *Phys. Rev. Lett.*, 76:2523, 1996.

[79] S. V. Dvinskikh and I. Furó. Combining PGSE NMR with homonuclear dipolar decoupling. *J. Magn. Reson.*, 144:142, 2000.

[80] S. V. Dvinskikh and I. Furó. Anisotropic self-diffusion in the nematic phase of a thermotropic liquid crystal by H-1-spin-echo nuclear magnetic resonance. *J. Chem. Phys.*, 115:1946, 2001.

[81] B. B. Mandelbrot. *Fractals: Form, Chance and Dimension*. Freeman, San Francisco, 1977.

[82] B. B. Mandelbrot. *The Fractal Geometry of Nature*. Freeman, San Francisco, 1982.

[83] H. O. Peitgen and P. H. Richter. *The Beauty of Fractals*. Springer-Verlag, Berlin, 1986.

[84] L. Pietronero and E. Tosatti, editors. *Fractals in Physics*. North-Holland, Amsterdam, 1986.

[85] P. Fischer and W. R. Smith, editors. *Chaos, Fractals and Dynamics*. M. Dekker, New York, 1985.

[86] S. Alexander and R. Orbach. Density of states on fractals: fractons. *J. Physique Lett.*, 43:625, 1982.

[87] R. Rammel and G. Toulouse. Random walks on fractal structures and percolation clusters. *J. Physique Lett*, 44:13, 1983.

[88] Y. Gefen, A. Aharony, and S. Alexander. Anomalous diffusion on percolating clusters. *Phys. Rev. Lett.*, 50:77, 1982.

[89] J. R. Banavar, M. Lipsicas, and J. F. Willemsen. Determination of the random-walk dimension of fractals by means of NMR. *Phys. Rev. B*, 32:6066, 1985.

[90] G. Jug. Theory of NMR field-gradient spectroscopy for anomalous diffusion in fractal networks. *Chem. Phys. Lett.*, 131:94, 1986.

[91] J. Kärger and G. Vojta. On the use of NMR pulsed field-gradient spectroscopy for the study of anomalous diffusion in fractal networks. *Chem. Phys. Lett.*, 141:411, 1987.

[92] E. Courtens and R. Vacher. Structure and dynamics of fractal aerogels. *Z. Phys. B. Condensed Matter*, 68:355, 1987.

[93] K. S. Mendelson. Nuclear magnetic relaxation in fractal pores. *Phys. Rev. B*, 34:6503, 1986.

[94] A. Blinc, G. Lahajnar, R. Blinc, A. Zidanšek, and A. Sepe. Proton NMR study of the state of water in fibrin gels and blood clots. *Bulletin of Magnetic Resonance*, 11:370, 1989.

[95] I. Oppenheim and P. Mazure. Brownian motion in systems of finite size. *Physica*, 30:1833, 1964.

[96] A. Lutti and P. T. Callaghan. Undulations and fluctuations in a lamellar phase lyotropic liquid crystal and their suppression by weak shear flow. *Phys. Rev. E*, 73:011710, 2006.

[97] A. Léon, D. Bonn, J. Meunier, A. Al-Kahwaji, O. Greffier, and H. Kellay. Coupling between flow and structure for a lamellar surfactant phase. *Phys. Rev. Lett.*, 84:1335, 2000.

[98] L. Courbin, J. P. Delville, J. Rouch, and P. Panizza. Instability of a lamellar phase under shear flow: Formation of multilamellar vesicles. *Phys. Rev. Lett.*, 89:148305, 2002.

[99] O. Diat, D. Roux, and F. Nallet. 'Layering' effect in a sheared lyotropic lamellar phase. *Phys. Rev. E*, 51:3296, 1995.

[100] O. Diat, D. Roux, and F. Nallet. Measurement of multilamellar onion dimensions under shear using frequency domain pulsed gradient NMR. *J. Magn. Reson.*, 187:251, 2007.

[101] S. L. Codd and P. T. Callaghan. Flow coherence in a bead pack observed using frequency domain modulated gradient nuclear magnetic resonance. *Physics of Fluids*, 13:421, 2001.

[102] R. Maier, D. M. Kroll, H. T. Davis, and R. Bernard. Simulation of flow in bead packs using the Lattice-Boltzmann method. *Physics of Fluids*, 10:60, 1998.